# ALUMINUM OXIDE AND TITANIUM DIBORIDE REINFORCED METAL MATRIX COMPOSITE AND ITS MECHANICAL PROPERTIES

**A THESIS SUBMITTED TO**
**THE GRADUATE SCHOOL OF NATURAL AND APPLIED SCIENCES**
**OF**
**MIDDLE EAST TECHNICAL UNIVERSITY**

**BY**

**AZİZ KURTOĞLU**

**IN PARTIAL FULFILLMENT OF THE REQUIREMENTS**
**FOR**
**THE DEGREE OF MASTER OF SCIENCE**
**IN**
**METALLURGICAL AND MATERIALS ENGINEERING**

**AUGUST 2004**

Approval of the Graduate School of Natural and Applied Sciences

_____

Prof. Dr. Canan Özgen
Director

I certify that this thesis satisfies all the requirements as a thesis for the degree of Master of Science

_____

Prof. Dr. Bilgehan Ögel
Head of Department

This is to certify that we have read this thesis and that in our opinion it is fully adequate, in scope and quality , as a thesis for the degree of Master of Science in Metallurgical and Materials Engineering.

_____ _____

Assoc. Prof. Dr. Ali Kalkanlı
Co-Supervisor

Prof. Dr. Naci Sevinç
Supervisor

Examining Committee Members:

Prof. Dr. İshak Karakaya (METU, METE) _____

Prof. Dr. Naci Sevinç (METU, METE) _____

Prof. Dr. Rıza Gürbüz (METU, METE) _____

Assoc. Prof. Dr. Hakan Gür (METU, METE) _____

Dr. Abdi Aydoğdu (MTA) _____

**I hereby declare that all information in this document has been obtained and presented in accordance with academic rules and ethical conduct. I also declare that, as required by these rules and conduct, I have fully cited and referenced all material and results that are not original to this work.**

Name, Last Name: Aziz Kurtoğlu

Signature :

# ABSTRACT


**ALUMINUM OXIDE AND TITANIUM DIBORIDE REINFORCED METAL MATRIX COMPOSITE AND ITS MECHANICAL PROPERTIES**

Kurtoğlu Aziz

M.S., Department of Metallurgical and Materials Engineering

Supervisor: Prof. Dr. Naci Sevinç

Co-Supervisor: Ass. Prof. Dr. Ali Kalkanlı

August 2004, 100 Pages

This study is on the production and testing of an aluminum metal matrix composite. Metal Matrix Composites can be produced in several different ways. In this study, an aluminum matrix composite is produced by direct addition of the reinforcement ceramic into the liquid metal. The ceramic reinforcement for this process was a mixture of $TiB_2$ and $Al_2O_3$ which was produced by means of a thermite reaction of reactants Al, $B_2O_3$ and $TiO_2$ all in powder form with their respective stoichiometric amounts. This ceramic mixture was ground to fine powder size and then added to liquid aluminum in small percentages. After casting and taking samples of unreinforced alloy and reinforced alloys, their tensile strength and hardness as material properties were measured and compared. Another issue is the wetting of ceramic particles by molten Aluminum. The aim of the experiments in general is to find a better way to produce a composite material with desired mechanical properties.



Keywords: Metal matrix composite, $TiB_2$, $Al_2O_3$, Stir casting, Pressure casting

# ÖZ

## ALÜMİNYUM OKSİT VE TİTANYUM DİBORÜR TAKVİYELİ METAL MATRİKSLİ KOMPOZİT VE MEKANİK ÖZELLİKLERİ

Kurtoğlu, Aziz
Yüksek Lisans, Metalurji ve Malzeme Mühendisliği Bölümü
Tez Yöneticisi: Prof. Dr. Naci Sevinç
Ortak Tez Yöneticisi: Doç. Dr. Ali Kalkanlı

Ağustos 2004, 100 sayfa

Bu çalışma bir alüminyum metal matriksli kompozit malzemenin üretimi ve test edilmesi üzerinedir. Metal matriksli kompozitler bir çok değişik yolla üretilebilir. Bu çalışmada, bir alüminyum matriksli kompozit, takviye seramiğin sıvı metale direkt eklenmesiyle üretilmiştir. Bu çalışma için gereken seramik takviye, reaksiyon girenlerinin hepsi karşılık gelen stokiyometrik miktarlarda toz halinde Al, $B_2O_3$ ve $TiO_2$ olduğu bir termit reaksiyonunca üretilmiş olan bir $TiB_2$ ve $Al_2O_3$ karışımıdır. Bu seramik karışımı ince toz boyutuna öğütülmüş ve yukarıda tanımlanan yöntemle küçük yüzdelerle sıvı Alüminyuma eklenmiştir. Bu yöntemle üretilen takviye edilmiş ve edilmemiş örnekleri döktükten sonra, malzeme özellikleri olarak çekme direnci ve sertlikleri ölçülmüş ve kıyaslanmıştır. Diğer bir konu da seramik parçacıkların erimiş Alüminyumla ıslanmasıdır. Deneylerin amacı genel olarak istenilen mekanik özelliklere sahip bir kompozit malzemeyi üretmek için daha iyi bir yol bulmaktır.

Anahtar Kelimeler: Metal matriksli kompozit, $TiB_2$, $Al_2O_3$, Karıştırmalı döküm, Basınçlı döküm

## ACKNOWLEDGMENTS

In the course of the production of this study, I would like to thank to Prof. Dr. Naci Sevinç for his patience and guidance at all times. For his suggestions and comments, I would also like to thank to Assoc. Prof. Dr. Ali Kalkanlı. Among the research assistants, Gökhan Demirci and Ender Keskinkılıç is gratefully acknowledged. Next, for their assistance and help, I would like to thank to the technical staff of the faculty. Lastly, I offer sincere thanks to my family who never lost faith in me during the course of this study, especially my mother.

TABLE OF CONTENTS

LIST OF FIGURES

FIGURES

# CHAPTER I

## INTRODUCTION

In recent years, there has been an interest in continously and discontinously reinforced MMC's in the way that these exhibit high strength, light weight and high stiffness properties over conventional alloys. MMC's in general consist of at least two components, namely matrix and the reinforcement. Matrix is mostly an alloy and the reinforcement is usually ceramic. The distinguishment of a MMC from an alloy is that, in an alloy, the second phase forms as a result of a eutectic or eutectoid reaction where in a MMC, the second phase and the matrix alloy is mixed together. Because of the different physical properties of the reinforcement, a few advantages of MMC's over conventional alloys are the combination of high strength, high elastic modulus, high toughness and impact resistance, low sensitivity to changes in temperature or thermal shock, high surface durability, low sensitivity to surface flaws, high electric and thermal conductivity, minimum exposure to the potential problem of moisture absorption resulting in environmental degradation and improved fabricability with conventional working equipment.

Early studies on MMC's were concentrated on continously reinforced MMC's. However, despite encouraging results, high cost of the reinforcement and the highly labor intensive manufacturing process restricted the effective use of these materials to military and highly specialized applications. On the other hand, in recent years, particulate reinforced composites attracted attention because of the availability of a range of reinforcements at competitive costs, successful development of manufacturing processes that utilize the production of MMC's with reproducible microstructure and properties and the availability of standart or near

standart metal working methods that can be used to form these materials. Furthermore, use of discontinous reinforcements has the advantage over fiber reinforced composites that it minimizes the problems associated with the latter such as fiber damage, microstructural heterogeneity, fiber mismatch and interfacial reactions. For some applications which are subjected to severe loadings or extreme thermal fluctuations such as automotive components, discontinously reinforced composites proved to show near isotropic properties with substantial increase in strength and stiffness compared to monolithic alloys. However, discontinously reinforced composites are not homogeneous and material properties are sensitive to the properties of the constituent, interfacial properties and the geometric shape of the reinforcement.

This study will examine the way to produce and the mechanical properties of a discontinously reinforced MMC. After some introductory data about MMC's, processing methods will be discussed in general and specifically, the way to produce a reinforcement and a composite and the resultant mechanical properties of this composite will be discussed.

# CHAPTER II

# LITERATURE SURVEY

## 2.1 Introduction

In this part, first of all, particulate reinforced metal matrix composites are introduced including matrix and reinforcement types, commercial availability plus examples from applications. After that, the processing methods to produce particulate reinforced composites is discussed. Some examples from the industry is also given in this part. Secondly, the thermite reaction by which the ceramic particle mixture is produced in this study is discussed. After that, the literature on the phenomena governing particulate reinforced metals is presented. These phenomena include the wetting of the ceramic particles by molten Aluminum focusing on $TiB_2$ and $Al_2O_3$ particles although separately, solidification of particulate reinforced metals, interfaces in particulate reinforced composites including the nature of the interfacial reaction between Aluminum and $Al_2O_3$, and porosity formation in reinforced metals. Additionally, the effect of particle size and shape on the mechanical properties of particulate reinforced metals and the strengthening mechanisms governing particulate reinforced metals is given.

### 2.1.1 Metal Matrix Composites

There are three types of metal matrix composites. These are:

- Particle reinforced MMC's
- Short fiber or whisker reinforced MMC's

- Continous fiber or sheet reinforced MMC's

These three types can also be grouped as discontinously reinforced MMC's and continously reinforced MMC's. Without going into further detail on the last two types, particle reinforced MMC's will be explained in terms of their use and advantages. While describing the processing methods of composites, main focus will be on the processing of discontinously reinforced composites which is related to this study.

Discontinously reinforced MMC's have some advantages over continously reinforced MMC's. First of all, they are inexpensive compared to continously reinforced MMC's. For example monofilament fiber reinforced composites are expensive as the production of these fibers is costly. Second, continously reinforced MMC's can be recycled most of the time. This is very difficult in the case of fiber reinforced composites. Also in many cases, near net shape casting can be performed during processing of discontinously reinforced composites. In addition to all of these, when the particle size distribution of the reinforcement is regular and fine, although this increases the cost, machining of produced parts is possible. Finally, continously reinforced composites are relatively much more isotropic than fiber reinforced composites.

### 2.1.2 Particulate Reinforced MMC's

Particle reinforced metals are produced by combining a metal or alloy with a finite volume fraction of roughly equiaxed particles mainly ceramic in order to improve the final properties. This is done mostly in order to increase the modulus, wear resistance or to lower the thermal expansion (of Aluminium). As an example, SiC reinforced Aluminium includes all of these. Generally, the improvements achieved is less extensive than fiber reinforced composites but they are cost effective, exhibit isotropic properties and compatible with most metalworking processes like as machining, deformation, processing and welding.

The primary driving force for the research and development on particulate reinforced MMC's is to produce a material with desirable properties without paying the cost of monofilaments, short fibers or whiskers.

Particulate reinforced MMC's have been produced for research at the universities since 1960. Powder metallurgical production of MMC's experimentally and in prototype quantities followed later and it resulted in the foundation of a powder metallurgical production base for these materials. One example to such producers is DWA which is a company that is currently active. A second development arised after this, including the use of molten metal which is much more cheaper than the solid metal, which gave rise to industrial production of material of good quality. This process and its first company (Dural) was purchased by Alcan and they produced these kinds of materials in the largest amount in the market under the trademark Duralcan.

Today these materials and their producers can be divided into two large groups namely powder metallurgical (P/M) and stir-cast particle reinforced metals. Additionally, in-situ processes in which the reinforcement is produced within the matrix by chemical means have been offered and used industrially (London and Scandinavian's $TiB_2$ reinforced Al). A fourth group appeared later in the 1990's which is the infiltration of preforms of particles used for the production of electronic substrates.

### 2.1.3 Metallic Matrix Types

There is a wide range of metals one can choose to use as the matrix of a MMC. Some important metallic matrixes and their properties is given below [1]:

**Aluminium Alloys**

Aluminium alloys are used mainly in the Aerospace Industry because of their low density and high strength, toughness and resistance to corrosion. To improve the

strength of Aluminium and its alloys without a loss in ductility, ceramic particles can be added forming a composite material.

**Titanium Alloys**

Titanium alloys are also used in the Aerospace Industry due to their low density. They retain strength to high temperatures and they have good oxidation and corrosion resistance. However, it is an expensive material.

**Magnesium Alloys**

Magnesium and its alloys are also light materials. Among others its density is the lowest, which is 1.74 $g/cm^3$. Magnesium castings are used in aircraft gearbox housings, chainsaw housings and electronic equipment.

**Copper Alloys**

Copper has a fcc crystal structure. It is used as an electrical conductor and has good thermal conductivity. It can be easily cast and worked. One major application in which copper is used as the matrix material is the production of niobium-based super conductors.

**Intermetallic Compounds**

Intermetallic compounds have extremely low ductility. This can be overcomed by some other methods but it is the best to use them as matrix materials to produce a composite to improve toughness.

### 2.1.4 **Reinforcements**

Particulate reinforced MMC's are being used for a range of industrial applications. Particulate is most commonly SiC or $Al_2O_3$ but others such as $TiB_2$, $B_4C$, $SiO_2$,

TiC, WC, BN, $ZrO_2$, W etc have been investigated [2] . During processing, chemical reaction can occur between the matrix and the particulate. For example SiC is reactive with Aluminum alloys where without the presence of Magnesium, $Al_2O_3$ is more stable in Aluminum alloys. However, when the matrix is Magnesium, this stability is reversed as Magnesium has high affinity for oxygen. When fibers are considered, generally coating is applied on the surface but particulate reinforcement is generally introduced into the matrix in virgin state. For structural applications, reinforcement particle size in diameter is in the range of 10 – 30 μm and about 10 – 30% volume percent of particles is used. Nevertheless, MMC's in which these values are outside these ranges are also used and available commercially, for example particularly fine particles and high volume contents. For electronic substrate applications, higher particle volume percentages are used, such as around 70% by volume.

### 2.1.5 **Commercial applications and availability**

Despite their improved mechanical and thermal properties of Metal Matrix Composites (MMC), the use of them in specific applications have been limited for a long time. Shortcomings such as complex processing routes and the high cost of the final product are the greatest barriers for the large scale industrial production of them. So, improvements in reinforcement fabrication and processing techniques are essential to increase the commercial availability of them. In recent years, significant efforts have been made in these areas and encouraging results have been obtained, which resulted in the increasing presence of large scale commercial applications. Some examples of currently produced parts (especially particulate reinforced metal matrix composites) are brace discs, drums, calipers or back – plate applications that are found in automotive braking systems. $TiB_2$ particle reinforced aluminum parts that are produced for aerospace and wear resistance applications can be found. Bicycle and golf components are also developing. Two examples of applications can be seen in figures 1 and 2.

Figure 3 [3] below shows a comparison of the performance and cost of Aluminum matrix composites. It can be seen that while the performance is increasing with the addition of ceramic to Aluminum, cost also increases.

**Figure 1. MMC Cylinder Liners / Honda Prelude**

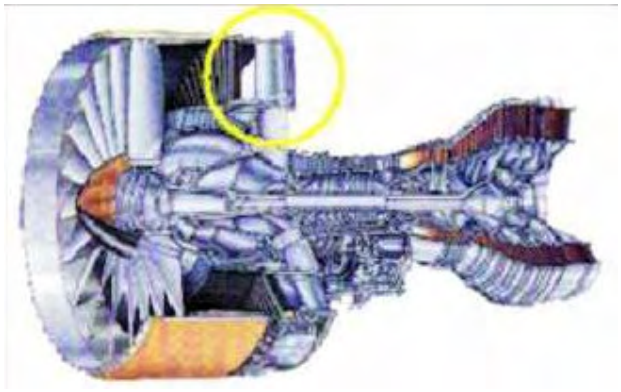

**Figure 2. Fan Exit Guide Vanes**

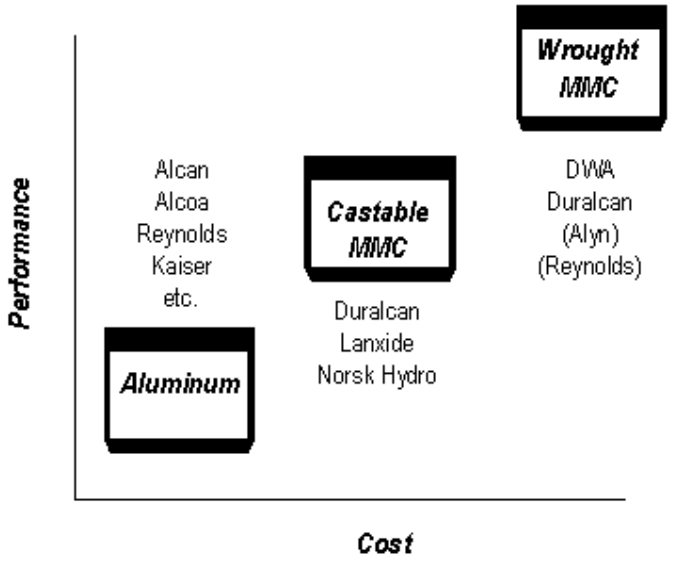


**Figure 3. Comparison of cost performance of Aluminum, Castable MMC and Wrought MMC.**

In the reference which the figure is referred to, low cost compositing processes are listed as direct powder metallurgy, improved stir casting and in situ compositing. In the case of improved stir casting, the benefits are listed as on site delivery of hot MMC to the foundry and low cost utilizing conventional equipment such as $0.15 – $0.30 per pound. The disadvantages are indicated as long mixing times unsuitable for reactive reinforcements and capital requirement for the dedicated MMC unit in the foundry.

### 2.2 Processing Methods

The need for high strength, lightweight and high stiffness materials led the industry and researchers to design and improve production techniques for MMC's. These techniques vary according to the state of the matrix or in general the process involved. There is a wide range of production techniques for composite materials but here the focus will be on the production of MMC's and especially particulate reinforced composites.

In the case of the production of MMC's, there are two phases present: matrix phase and the reinforcement phase. The matrix is a metal or an alloy of a base metal and the reinforcement is generally ceramic. If a material is to be called as a MMC, the matrix and reinforcement should be only mechanically mixed, not chemically, otherwise the product will be an alloy, not a composite material. Moreover, a composite is distinguished from other materials where the second phase forms as a particulate and a phase seperation such as a eutectic or eutectoid reaction occurs.

In recent years, particulate reinforced MMC's attracted considerable attention due to the availability of a wide range of reinforcements at low costs. The attractive properties of particulate reinforced MMC's also come from the fact that succesful manufacturing processes have been developed to produce MMC's with reproducible microstructure and properties and there exists standart and near standart metalworking methods that can be utilized to form these materials. Furthermore, use of discontinuous reinforcements minimizes problems that can be seen during the fabrication of continuously reinforced composites such as fiber damage and microstructural inhomogeneity.

The processes can be grouped according to the temperature of the metallic matrix during the processing. So the processes can be divided into two main categories: Solid state processes and liquid state processes. In addition to these, there are two phase processes where the matrix is between liquidus and solidus and these are called two phase (solid-liquid) processes.

### 2.2.1 Solid State

Solid state processing involves a number of steps to final consolidation. These processes utilize the fabrication of particulate reinforced MMC's from blended elemental powders. Two methods fall into this category: Powder metallurgy and high energy rate processing.

#### 2.2.1.1 Powder Metallurgy

Solid state processes involve the blending of rapidly solidified powders with particulates, platelets or whiskers using a number of steps. These are sieving of the rapidly solidified powders, blending with the reinforcement phase, pressing up to 75% density, degassing and and final processing by extrusion, forging, rolling or some other hot working method. The P/M process has been developed succesfully for some commercial applications. Two commercial applications, Alcoa and Ceracon processes are available. Final consolidation is achieved by hot extrusion in the Alcoa process whereas in the Ceracon process final densification is achieved by hot pressing. For example P/M processed Al-SiC MMC's possess high strength relative to the MMC's produced by conventional liquid state methods, however their elongation is somewhat lower.

The P/M method produces parts which are superior in microstructural requirement to the parts produced by conventional liquid state methods. This is due to the rapid solidification of powders which leads to the development of matrix materials which have compositional limits that can not be reached by the thermodynamics of conventional solidifying methods. Another superiority of the P/M method to the conventional casting and liquid metal infiltration methods is that, particles are more homogeneously distributed by this method.

The limitations of P/M method are:

- Limited availability of metal powders
- High cost of metal powders
- High cost of hot pressing

#### 2.2.1.2 High Energy Rate Processing

High energy high rate processing is a technique that can be succesfully employed to consolidate metal powders containing a fine distribution of ceramic particles. In this technique, the consolidation of the powder mixture is achieved by applying

high energy, either mechanical or electrical, over a short period of time. In the case of electrical energy, the high energy high rate pulse heats the conducting powder rapidly in a die with cold walls. The short time approach enables the producer to control phase transformations and the degree of coarsening which is not possible in the case of conventional techniques.

#### 2.2.1.3 Diffusion Bonding

Diffusion bonding is a common solid state welding technique. Major advantages of this technique are the ability of using a wide variety of matrix materials and control of fiber orientation and the volume fraction of the fiber. The disadvantages are processing times of several hours and high cost of processing temperatures and pressures.

Diffusion bonding process has numerous variants but in all cases high temperature and pressure is applied simultaneously. This process is for fiber reinforced composites so without going into further detail, only the basic principles will be explained. In a common case, metal alloys are in the form of sheet and reinforcement material is in the form of fibers and these are stacked in arrays in a predetermined order. Bonding occurs by press forming directly. After bonding, as a secondary process machining is done. Another method includes the application of the matrix material on the reinforcement using various coating methods such as plasma spraying, chemical coating, electrochemical plating and plasma vapor deposition (PVD). Plasma spraying is the simplest method of low cost that can be able to produce of sheets of large width with good adhesion between the matrix and the reinforcement. The preform is then hot pressed to enchance the density of the composite by removing voids and to improve the strength by causing some plastic deformation in the matrix. Diffusion bonding is better in vacuum conditions than in atmospheric conditions.

Among other methods, diffusion bonding of fiber arrays with matrix alloy powder or matrix foil is the most effective. This is due to the ability of the reinforcement

to deform plastically which inhibits fiber cracking during processing allowing secondary plastic deformation of the composite.

### 2.2.2 Liquid State

As it is said before, processing of MMC's can be generally divided into two categories such as solid state and liquid state. Solid state techniques has been given above and now liquid state techniques will be explained. Majority of the commercially useful applications are done by liquid state methods because of the advantages of these processes over the solid state processes. First of all, liquid metal is less expensive than solid powders and it is also easier to handle. The product can be shaped into the desired shape by using conventional casting methods. However, there is a lack of reproducibility of these materials due to the incapability to control the processing parameters and the unwanted chemical reactions at the metal reinforcement interface. For these reasons, these processes are limited to low melting point alloys although some intermetallic matrix composites can now be produced commercially.

Liquid state processes can be divided into four categories on the basis of them to physically combine the matrix and the reinforcement [4]. These are:

1. **Melt Stirring (Dispersion)**
2. **Infiltration**
3. **Spraying**
4. **In-situ**

There are some phenomena covering these processes such as wetting and interfacial reactivity but these phenomena will be described in parts 2.3 and 2.5.1 of this study separately focusing on the melt stirring method which is closely related to this study. Also, related to the solidification, particle engulfment will be explained in terms of the melt stirring method as a seperate part. Before these, melt stirring method is discussed as a processing method.

### 2.2.2.1 Melt Stirring

In this process as described in figure 4, reinforcement (ceramic) is added in loose powder form to the molten metal. Ceramic reinforcements exhibit poor wetting in the liquid metal, so mechanical force is needed to incorporate the particles to the melt and this is usually done by stirring. Melt stirring method is currently the most inexpensive method and leads to conventional production of material by applying secondary processes such as casting or extrusion.

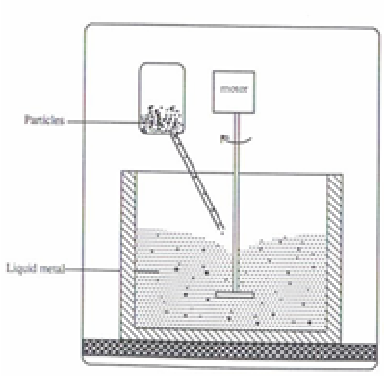


**Figure 4. Schematic illustration of a typical melt stirring process**

The simplest process is the vortex method which is the vigorous stirring of the molten metal and adding the particles to the vortex. Skibo and Schuster [5,6] patented a process in 1988 in which SiC particles are incorporated to molten aluminum under vacuum with a specifically designed propeller. This method has the advantage of minimizing the incorporation of impurities, gases and oxides into the melt by minimizing the vortex and because of the vacuum. Such types of composites are now commercially produced by Duralcan company. Other mixing methods include the bottom mixing process and the injection of particles under the surface of the melt using a carrier gas such as argon. The success of the process depends on the control of undesirable events such as porosity resulting from gas entrapment during mixing, oxide inclusions, reaction between the metal and the reinforcement due to long contact times and particle clustering and agglomeration.

Particle mixing of metals can also be performed when the metal temperature is kept between solidus and liquidus. This process is known as compocasting and it is a consequence of the rheocasting process applied for unreinforced semi solid slurries. The advantage of this process is that, migration of particles in the metal is prevented by the solid phase and the increase of the viscosity of the melt. Another method for mixing particles with semisolid metals is thixomolding where metal pellets and particles are extruded through an injection molding apparatus [7].

Among the governing phenomena, particle incorporation is important as the particles are not readily wet by the molten metal due to the difficulty of replacing the particle gas interface with the particle liquid interface as well as breaking the oxide layer. An equation given by Ilegbusi and Szekely in 1988 [8] gives the force balance on a partially immersed particle in the melt in the vertical direction which is indicated below:

$$\Sigma F = F_B + F_G + F_H + F_S + F_E \text{ ; where}$$

**$F_B$ = Buoyancy force on the immersed part**

**$F_G$ = Gravity on the whole particle**

**$F_H$ = Hydrostatic pressure of the liquid above the contact area**

**$F_S$ = Vertical component of the surface tension**

**$F_E$ = Drag force caused by the motion of the liquid**

**Equation 1.**

This equation however does not take into account some events such as the interaction of the particles between themselves, the effect of the shape of particles and the presence of a thick oxide layer on the melt surface. Nevertheless, it is also indicated that in case of electromagnetically stirred melts, small particles are more

difficult to engulf and high melt velocities are required when the ceramic reinforcement is not wetted by the molten metal, which agrees with the equation Also, if high shear is applied at the interface between the particles and the melt, particles can be engulfed. The shearing action helps to break the oxide layer and spreads the particles on the surface and this effects the homogeneous distribution of particles in the melt. Finally, best results are gained when there is no gas in the melt, meaning that the vortex at the surface is minimized and when a vacuum condition is present.

Other phenomena governing melt stirring process are fluid flow and particle migration. Particle migration will be discussed in part 2.4 in this study so here it will only be discussed introductorily. On the other hand, fluid flow is another important subject and it will be discussed here shortly.

Unreinforced metals have a viscosity about 0.01 poise which is similar to water and they can be considered as Newtonian fluids. This means that their viscosity is independent of shear rate and decrease with temperature. When ceramic particles are added to these metals, their viscosity increases due to the interaction of particles with each other and the matrix, creating more resistance to shear stress. Typical values of viscosity in this case is in the range of 10 – 20 poise for Al alloy reinforced with 15 vol% SiC particles. It is a fact that viscosity is a function of reinforcement volume percent, particle size and shape. An increase in volume fraction or a decrease in size increases the viscosity of the slurry. This puts a limit to the practically reachable reinforcement amount up to about 30% in volume. The temperature is another factor which effects dispersion mixing while the alloy temperature is between liquidus and solidus. The metal particulate slurries exhibit a non newtonian behavior in both of the cases where the temperature is above liquidus or between liquidus and solidus. Their viscosity changes about an order of magnitude as shear rate increases and it is also observed experimentally that they are thixotropic, meaning that when the shear rate is changed, the viscosity of the slurry changes slowly to reach the new steady state value. This behavior can not be fully understood yet but it implies that clustering and declustering of particles play a major role in this process. Another factor, interfacial reactions also increase the

viscosity of the slurry as because the reaction products have different density, they break and change the morphology of the reinforcement.

In the semi solid temperature range, composite slurry behavior is explained by the same way as unreinforced melts. When shear is applied, there is a change in the morphology of the solid phase as a result of dendrite fragmentation, rippening and abrasion and collision and coalescence of solid particles. As quoted by reference 4, Mada and Ajersch developed an analytical model of thixotropic behavior in semi solid composite slurries. They concluded that particle addition has little influence on thixotropic behavior and the major factor is the primary solid phase. In an other study by Moon et al. which is also quoted by reference 4 it is observed that viscosity of slurries composed of SiC particles combined with an aluminum alloy in the semisolid temperature range was lower than that of unreinforced slurry with the same volume % of solid. This can be explained by the location of ceramic particles between dendrite arms preferentially, limiting the contact and agglomeration of dendritic solid particles.

The last phenomena governing melt stirring method is the particle migration. This subject is extensively investigated in the part 2.4 of this study, so only a brief introduction will be given here. After mixing, the composite might be at rest before solidification. Here, the issue of the density difference between the particles and the melt arises. For high reinforcement volume fractions, sedimentation of particles is affected by the size distribution and interactions of particles. In order to produce homogeneously reinforced composites, an understanding of the interaction of the growing solid metal and the particles is essential. When particles encounter a moving solid liquid interface, they may either be engulfed in the solid or pushed by the interface and collect in regions which solidify last, for example in the interdendritic regions. It is experimentally observed that there is a criticial velocity, $V_c$ of the interface under which particles are pushed and above which they are engulfed. There are some models governing this phenomena but they are not easy to compare with the experimental results as the parameters do not vary independently and castings do not solidify at steady state as assumed by these models.

### 2.2.2.2 Infiltration

Infiltration processes occur when molten metal alloys are infiltrated through a porous preform of ceramic particles. An example is given in figure 5. Infiltration process is not new, it has been used for many years in powder metallurgy to strengthen porous steel parts with copper. However, there is a major difference between infiltration of solid metal by liquid metal and ceramic preforms by liquid metal, that is liquid metals do not spontaneously wet the ceramic. For this reason, external pressure must be applied to force the liquid metal into the preform. This preform can be applied either by using an inert gas or a mechanical device. The parameters in infiltration processes are the initial composition, morphology, volume percentage and temperature of the reinforcement as well as the initial composition and the temperature of the infiltrating metal and the nature and the magnitude of the external force applied to the metal if there is such force present.

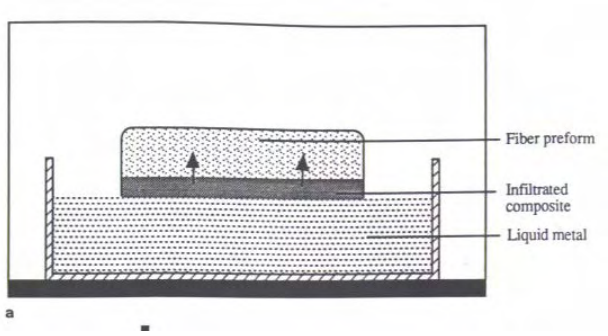


**Figure 5. A general illustration of an infiltration process**

Infiltration processes is classified according to the nature and magnitude of the external force applied during infiltration in this study. The classification is as follows:

1. **No External Force**
2. **Vacuum Driven Infiltration**

3. **Pressure Driven Infiltration**
4. **Other Forces**

#### 2.2.2.2.1 No External Force

In some specific cases, the metal spontaneously wets the reinforcement. Specifically tailored chemistry and conditions can be used to produce spontaneous infiltration. Examples are infiltration of copper into tungsten which is driven by the direct wetting of metals, infiltration of reinforcements into molten aluminum by direct coating of reinforcements by nickel or the Lanxide Primex process™ in which Al Mg alloys infiltrate ceramic preforms at temperatures between 750 and 1000°C in a nitrogen rich atmosphere. There are other processes namely reactive spontaneous infiltration processes which result in composites reinforced with borides and nitrides [9,10] .

#### 2.2.2.2.2 Vacuum Driven Infiltration

Vacuum infiltration is a process where a hydrostatic pressure of one bar drives the metal matrix into the preform under vacuum conditions. In some cases, the vacuum can be self generated, for example reaction of Mg with oxygen or air in the preform.

#### 2.2.2.2.3 Pressure Driven Infiltration

Pressure driven infiltration is used to overcome poor wetting conditions which use work to force the metal into a preform. Wetting in this case can be quantified by measurement of the minimum pressure $\Delta P$ that must be applied on the metal to combine the two phases at a very small velocity. When $\Delta P$ is negative, it can be said that the metal wets the reinforcement and spontaneous infiltration occurs as described above such as wetting of tungsten fibers with copper. However, this is

not the case in ceramic reinforced metals, so positive pressure must be provided to create the composite. In reference 11, ΔP is given below as:

$$\Delta P = S_f (\sigma_{SL} - \sigma_{SA})$$

**$\sigma_{SL}$ = Surface energy per area of the solid liquid interface**

**$\sigma_{SA}$ = Surface energy per area of the solid air interface**

**$S_f$ = Surface area of interface per unit volume of the matrix**

**Equation 2.**

In this case, it is apparent that the work of immersion is the dominant factor in this process. However, this value of ΔP is a lower bound for the pressure required for the infiltration because irreversible energy losses are involved in the process. These energy losses arise from interfacial reactions and mechanics of the wetting of a porous medium. Mechanical irreversibility in wetting of preforms is seen by hysteresis of drainage imbibation curves where the volume fraction of liquid is plotted versus pressure applied on a liquid. This hysteresis occurs because energy is mechanically lost during infiltration. As a consequence of this, wetting angles below 90 does not imply that infiltration process will be spontaneous. As indicated above, primary purpose of applying pressure is overcoming capillary forces but applying pressure has some benefits such as increased processing speed, control over chemical reactions, refined matrix microstructures and soundness of product due to the feeding of solidification shrinkage.

Pressure is applied either by a gas or mechanically. In the case of gas pressure, an inert gas such as argon is used to push the metal into the preform. A typical sketch of the process is given in figure 6. The process was first patented by in 1970 [12] and has been used widely since to produce reinforced aluminum alloys. Normally, pressure ranges from 1 to 10 Mpa is used but the use of higher pressures up to 17

Mpa has also been investigated for aluminum matrix composites. However safety issues become a limiting factor in this case.

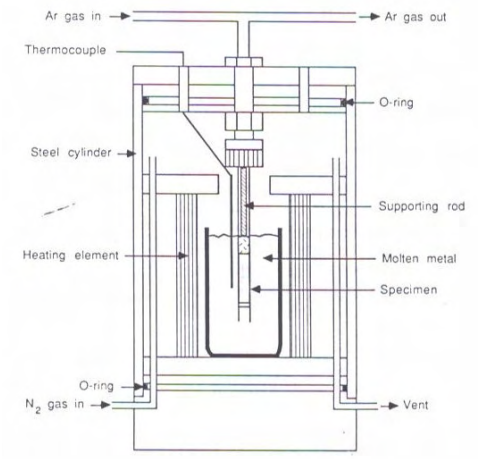


**Figure 6. An illustration of a pressure infiltration process**

The technique which utilizies mechanically applied pressure involves the use of the piston of a hydraulic press that applies a force on the molten metal subsequently maintained during solidification. In this case the pressures are higher than they are in gas driven processes, ranging from 10 to 100MPa. This type of infiltration process is the most widely investigated for commercial applications since it has been directly adapted from established processes used to cast unreinforced metals such as squeeze casting in which the piston constitutes part of the mold. Composites produced by this method generally exhibit a pore free matrix. However, application of pressure might cause preform damage during infiltration which is also observed experimentally.

2.2.2.2.4 **Other forces**

Alumina preforms have been infiltrated by Al Si alloys under low pressure with the assistance of vibrations at a frequency up to 3 kHz. Centrifugal casting methods have been used to produce tubularly reinforced metals. Also a new process has

been developed which uses electromagnetic body forces to drive molten metal into a preform.

The major advantage of infiltration processes in general is that they allow near net shape production of parts. Together with this, if cold dies and reinforcements are used and if high pressures are applied during solidification, matrix reinforcement reactions can be minimized and defect free (no porosity) matrix microstructures can be obtained. The limitation of infiltration processes is that the reinforcement needs to be self supported either as a bound preform or as a dense pack of particles and fibers. Final product heterogeneity might result from preform deformation during infiltration. Also, expensive tooling might be observed if high pressures are used.

#### 2.2.2.3 Spraying

In these processes, which is schematically represented in figure 7, metal droplets are sprayed together with the reinforcement and collected on a substrate where the composite solidification takes place. As an alternative to this, the reinforcement might be placed on the substrate and molten metal might be sprayed on it. These processes have been utilized for the production of unreinforced metals for the last 20 years because high solidification rate of droplets produces materials with little segregation and with refined grain structure. Various composite spray processes differ from each other by the method of spraying the metal and by the way reinforcement is mixed with the metal. Critical parameters are initial temperature, size distribution and the velocity of the metal drops and the velocity, temperature and feeding rate of the reinforcement and the position, temperature and the nature of the substrate. In most spray deposition processes, gases are used to atomize the molten metal into droplets of generally up to 300μm in diameter. The particles can be injected within the droplet stream or between the liquid stream and the atomizing gas as in the Osprey process developed by Alcan International. Osprey process has been scaled up for the production of 100 kg ingots of SiC reinforced Al

alloys. Other methods have been developed to produce molten metal drops from aluminum. These methods include arc melting, flame spraying or a combination of both. Plasma torches are used to melt and spray metal powders, various low and high temperature matrices such as Al alloys and $Ti_3Al$ or $MoSi_2$ reinforced with SiC, TiC or $TiB_2$ particles are prepared by this method (plasma spraying).

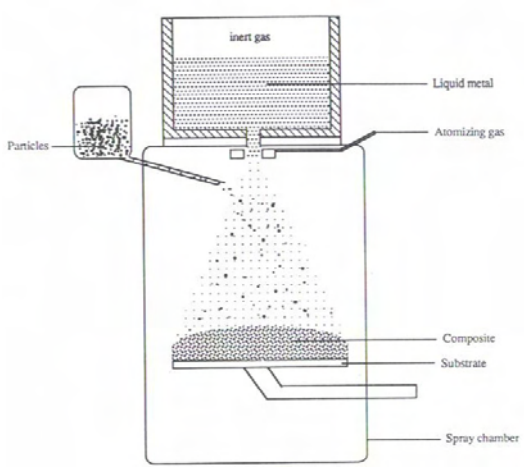


**Figure 7. Figure representing a spray deposition process**

An advantage of spray deposition techniques is the resulting fine grained matrix microstructures with low segregation. Also, interfacial reactions are minimized as the liquid metal and reinforcement contact only briefly. Simple forms such as ingots or tubes may be produced by this method although these lack in part shape versatility. Another disadvantage is the amount of porosity which is generally a few percentage in case. There is also the need to further process these materials. Spray deposition is not economical as dispersion and infiltration processes because of the high cost of the gases used and the large amount of powder waste which has to be disposed.

#### 2.2.2.4 In situ Processes

In these processes, as the name implies, the reinforcement phase is formed in situ. The composite material is produced in one step from a starting alloy, thus the difficulties encountered in combining separate components as in the production of typical composites are avoided. Recent research has been focused on in situ composites because reinforced intermetallic alloys can be produced by controlled solidification or by other in situ processes such as chemical reaction between a melt and a solid or gaseous phases. Unidirectional solidification of an eutectic alloy can also result in one phase being distributed in the other in the form of fibers or ribbons.

Some examples obtained from alloy solidification include Fe-TiC composites produced from solidification of Fe Ti C melts, TiB rods in TiAl matrices from solidification of melts containing γ-TiAl, Ta and B and TiC/Ti composites from mixtures of Ti and C with Al additions.

The XD process is an example that uses an exothermic reaction between two components to produce a third component. Such processing techmiques are referred to as self propagating high temperature synthesis (SHS) processes. Figure 8 illustrates a typical SHS process to make an MMC. The XD method is developed by Martin Marietta Corporation for producing ceramic particle reinforced metallic alloy. In this process, Ti, B and Al powders are heated to a temperature of 800°C and react to form $TiB_2$. By this reaction synthesis, generally a master alloy containing a rather high volume fraction of reinforcement is obtained first and then this alloy is mixed and remelted with the base alloy to produce a desirable amount of reinforcement. Other than this process, another example is the production of a $TiB_2$ reinforced composite where cryolite salts react with molten aluminum to produce the reinforcement. A scheme of this process is given in figure 9 In this process, the average particle size is 1-2μm giving additional strength to the material by dispersion hardening.

Another way to produce in situ composites is to react molten metal with a gas. An example is Lanxide's Dimox process in which the metal is directionally oxidized to produce a NNS composite. The typical process involves raising an aluminum melt to a high temperature with additions such as Mg so that the alumina skin produced becomes unstable by the formation of a porous compound and the metal moves by capillary action into an array of ceramic particles. In a study on the Dimox process by Tang and Bergman [13], it was observed that when the Al alloy is doped by $SiO_2$ on the top, the incubation time is substantially decreased by retarding the

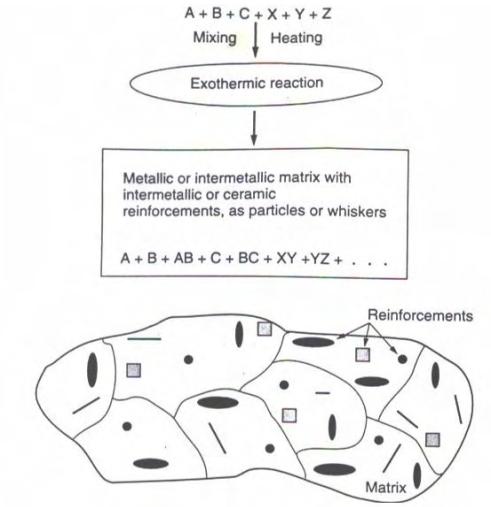


**Figure 8. A typical in situ (SHS) process**

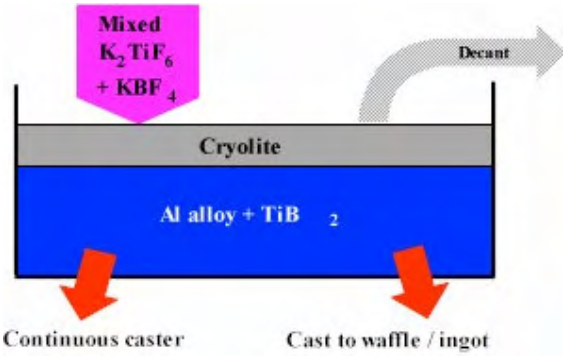


**Figure 9. Schematics of the mixed salt process**

reaction $Mg^{+2} + O_2 = MgO$ and promoting the reaction $MgO + Al^{+3} + O_2 = MgAl_2O_4$ which makes the reaching of Al microchannels to the free surface to start the bulk oxidation of Al much easier as this last product destables the alumina skin on the Al surface. Another example where the in situ composite is produced with the reaction with a gas includes the formation of TiC reinforced Al Cu alloys by bubbling $CH_4$ and Ar gas through a melt of Al Cu Ti. This gas injection method can be used to prodcue a wide array of carbide and nitride reinforced alloys.

The major advantage of in situ composite materials is that, the reinforcing phase is homogeneously distributed and spacing or size of the reinforcement may be adjusted by the solidification or reaction time. However, in practice the solidification rate is limited to a range of 1-5 cm/hr because of the need to maintain a stable growth front which requires a high temprerature gradient. Also the kinetics of the process in the case of reactions and the shape of the reinforcing particles is difficult to control.

### 2.2.3 Summary of Processing Methods

Finally, a summary of processing methods is given as headlines below together with a diagram (figure 10) showing primary and secondary states of production of materials by these processing methods [14]:

**Liquid State Processes**

- stir-casting
- compocasting
- semi-solid forming
- thixocasting
- infiltration
- spontaneous infiltration
- forced infiltration
- pressure infiltration
- vacuum infiltration

- gas pressure infiltration
- pressure assisted investment casting
- mechanical pressure infiltration
- squeeze casting infiltration
- pressure die infiltration
- centrifugal infiltration
- ultrasonic infiltration
- Lorentz force infiltration
- spray casting

**Solid State Processes**

- MMC diffusion bonding
- Foil-fibre-foil method
- wire winding
- powder cloth method
- powder consolidation
- MMC sintering
- MMC liquid phase sintering
- MMC hot pressing
- MMC cold pressing
- MMC hot isostatic pressing
- MMC cold isostatic pressing
- MMC powder rolling
- MMC powder extrusion
- MMC powder forging

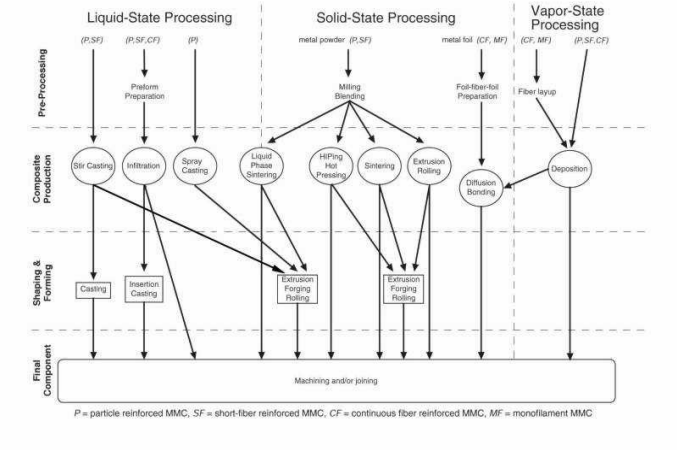


**Figure 10. Diagram showing primary and secondary stages of processing of MMC's**

## 2.3 Thermite Reaction and Its Use in the Production of the Reinforcement

Thermite reactions are self sustaining highly exothermic reactions which use their released thermal energy to propogate. Generally, the reaction is initiated at one end of a compact powder mixture and it continues up to the end of the compact converting all reactants into products. Thermite reactions have the advantage of forming ceramics with low cost. This low cost is due to the fact that cheap raw materials such as oxides can be used. Also high reaction temperatures permit rapid firing only without the use of furnaces.

The classical thermite reaction is the iron oxide aluminum thermite reaction in which adiabatic temperatures up to 3000°C can be obtained. This reaction requires only the reactants iron oxide and aluminum and a temporary heat source or ignition temperature of 1000C. This temperature is sufficient to melt both products, iron and aluminum oxide which lets the seperation of these phases. This reaction is particularly important as it has a long history in which it is used for a wide range of industrial applications. Steel castings of up to 450 kg have been produced by this method.

Other than the classical thermite reaction, some advanced ceramics such as SiC, $B_4C$, $Al_2O_3$ and SiC, and MgO and $B_4C$ is fabricated through thermite reactions. The feasibility of producing various ceramics by Aluminum based thermite reactions was investigated elsewhere. Also the effect of $TiB_2$ additions to the reactant mixtures during the production of a $Al_2O_3$ - $TiB_2$ composite was studied before.

Apart from all of these, relevant to this study, the production of $TiB_2$ and $Al_2O_3$ by utilizing a thermite reaction has been studied by Logan [15,16]. The aim in these studies is to produce $TiB_2$, which is an expensive material to produce commercially because of the extreme processing and fabricating conditions. Some methods were used before to produce $TiB_2$. Fused mixtures of $TiO_2$, $B_2O_3$ and the oxides and fluorides of calcium, magnesium or sodium have been electrolyzed

to yield $TiB_2$. Logan also studied particle particle interactions during oxidation reduction type self heating synthesis (SHS) reactions using laser exposure. The aim of this study was to determine the reaction path in the $TiB_2 – Al_2O_3$ formation reaction using differential thermal analysis (DTA) and x-ray diffraction.

The thermite reaction to obtain $TiB_2$ and $Al_2O_3$ from reactants Al, $TiO_2$ and $B_2O_3$ is as follows:

$$10\ Al + 3\ TiO_2 + 3\ B_2O_3 = 5\ Al_2O_3 + 3\ TiB_2$$

The $\Delta H$ of this reaction at 298K is calculated from references [17,18] and it is equal to –618.8 kcal, which is also equal to -2589059.2 joules. This indicates that the reaction is highly exothermic and it produces a local heat zone, reaching adiabatic flame temperatures above the melting point of $Al_2O_3$. The enthalpy curve of the reaction is given in figure 11.

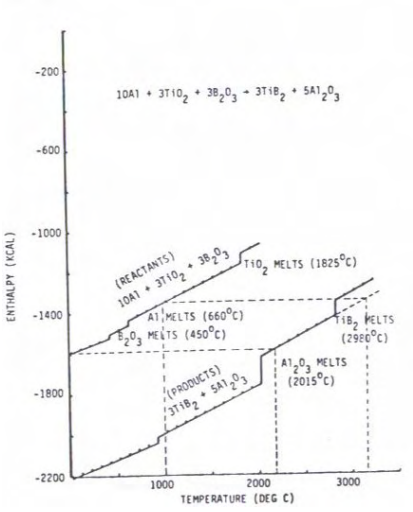


**Figure 11. Enthalpy diagram of the thermite reaction $10Al + 3TiO_2 + 3B_2O_3 = 3TiB_2 + 5Al_2O_3$**

In the study of Logan and Walton [15], it is observed by SEM and EDXRA analysis that a possible phase separation occured in the microscopic scale but not on the macroscopic scale. There were also areas of eutectic microstructure where Ti and B were the elongated structures and Al and O were the matrix. This observation indicates the fact that melting and recrystallization occurs during the reaction which is consistent with the fact that high adiabatic flame temperatures are reached.

As mentioned before, one of the properties of thermite reactions is that, when they are ignited, they can self propagate. It has been observed that when the reactant powder mixture is in loose form, mixtures containing coarse $TiO_2$ tend not to ignite. Pressed pellets tend not to ignite when the sample contains fine $TiO_2$, coarse $B_2O_3$, coarse Al or coarse $TiO_2$, fine $B_2O_3$ and fine Al. This illustrates the effect of the powder sizes on the reaction.

The ignition of the samples were also investigated by the same authors and figure 12 shows the typical ignition curves produced by the reaction when the powder is in loose form. The furnace was preheated up to 1260ºC and the samples were allowed to heat at a constant rate. It can be seen from the figure that in the case of loose powder form samples ignition occured during the melting of aluminum, at about 800-870ºC, however in the case that the sample is in compact form, this temperature was higher, around 980, 1100ºC as it can be seen from figure 13. It can also be observed from both of the figures that samples containing fine Al ignited at lower temperatures in both loose powder and pressed pellets. It was also observed by X-ray diffraction that the reaction went into completion in all cases where different particle sizes were used, compaction were different (loose form or pressed pellets) and ignition was from the room temperature or it started in a preheated furnace.

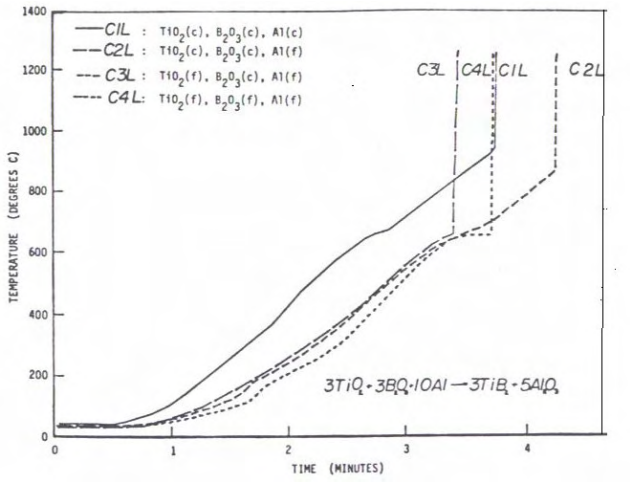


**Figure 12. Typical ignition curves of the thermite reaction in the case of loose powder form reaction mixture (The subscripts ( c ) and ( f ) refer to coarse and fine powder form)**

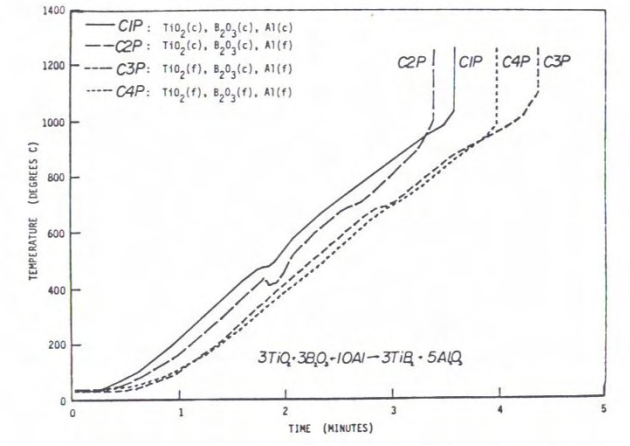


**Figure 13. Typical ignition curves of the thermite reaction in the case of packed form reaction mixture (The subscripts ( c ) and ( f ) refer to coarse and fine powder form)**

If all of these is summarized, the following conclusions is derived for the aluminothermic reaction:

- **Particle size**
  Lower ignition temperatures can be obtained when the particle size of Al is fine in both cases where the powder is in loose form or compacted.
- **Compaction**
  Loose powder ignites at lower temperatures than compacted powder in all cases
- **Temperature at ignition**
  In both cases where the sample is ignited from room temperature or in a preheated furnace, complete reaction is observed.
- **Atmosphere**
  Under air atmospheric pressure, $TiB_2$ is completely formed which is an indication that the reaction is complete.
- **Phase Separation**
  Phase separation of $TiB_2$ and $Al_2O_3$ occurs on a microscopic scale.

The mechanism of this reaction has been investigated [16]. In this study, the reaction is investigated under two different conditions where the first is the condition that the reactant powder mixture was under argon atmosphere and the second is the one that the reaction took place under air. Differential thermal analysis (DTA) and X-Ray diffraction analysis were performed and samples were heat treated to examine the phase changes occuring. DTA analysis shows clearly that an endothermic peak occured at the melting point of aluminum (figure 14) in both conditions. The broad exotherm at around 800ºC indicates the oxidation of Al. The broad nature of this curve arises from the fact that $Al_2O_3$ maintained a gas impermeable layer over the liquid Al and the thermal expansion mismatch between the layer and liquid resulted in periodic cracking of the $Al_2O_3$ layer and continous oxidation. For the mixture under Ar atmosphere after heating up to 1072ºC, $TiB_2$

formed with $Al_2O_3$ with a trace amount of $Al_{18}B_4O_{33}$. In this study, it is indicated that the exotherm at 1060ºC corresponds to the reaction,

**$AlTi_3 + 6B = 3\,TiB_2 + Al$**

but in the present study, the existence of this reaction could not be seen and a different conclusion is obtained which is told in part 4.1. The $TiB_2$ forming exotherm at 1060C is thus restricted to happen just after the formation of B by this reaction. With heat treatment to 1400C, the relative percentage of $Al_2O_3$ decreased while of $TiB_2$ and $Al_{18}B_4O_{33}$ increased. It is observed that this increase is due to the fact that the product $Al_2O_3$ and $AlTi_3$ acted as reactants to facilitate more formation of $TiB_2$ and $Al_{18}B_4O_{33}$. For the case where the atmosphere was air, it was observed that after heat treatment at 1081ºC, a small amount of $TiB_2$ was formed together with $Al_2O_3$ and significant quantities of unreacted Al and $TiO_2$ reactants was detected. The lack of reaction up to this temperature can be as a result of the formation of $Al_2O_3$ reaction barriers on Al.

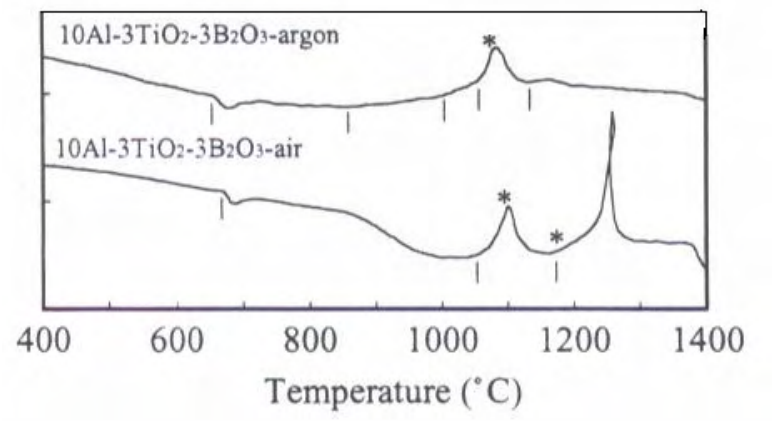


**Figure 14. DTA (Differential Thermal Analysis) diagrams of the thermite reaction under argon and air atmospheres**

Infact, it is seen that bulk ignition of this mixture can be succesfully performed to convert all reactants into products forming a $TiB_2$ $Al_2O_3$ composite. All of these treatments described above were performed in slow heating and cooling rates (50ºC/min) so this can be explained depending on the fact that in the bulk ignition process, the heating and cooling rates is so rapid that oxidation of reactants or formed $TiB_2$ can not occur.

Finally, the mechanism of the reaction of formation of the $TiB_2$ and $Al_2O_3$ component mixture is proposed by the authors as below:

$$6\,Al + 3B_2O_3 = 3\,Al_2O_3 + 6B$$
$$3\,TiO_2 + 5Al = AlTi_3 + 2Al_2O_3$$
$$AlTi_3 + 6B = 3TiB_2 + Al$$

---

$$10\,Al + 3\,B_2O_3 + 3\,TiO_2 = 5\,Al_2O_3 + 3\,TiB_2$$

However, in the present study, it will be shown that this is not the case.

## 2.4 Wetting Phenomena and Wetting of Ceramic Particles by Molten Metals in the Production of MMC's

Wetting and spreading are well defined thermodynamic processes but their use is both diverse and inconsistent [19]. In the past, wetting properties were measured experimentally from the contact angle and surface tension of the liquid by using the famous Young's equation:

$\gamma_{sv} - \gamma_{sl} = \gamma_{lv} . \cos\theta$

**$\gamma_{sv}$ = Solid vapor surface tension**

**$\gamma_{sl}$ = Solid liquid surface tension**

**$\gamma_{lv}$ = Liquid vapor surface tension**

**$\theta$ = Contact angle**

**Equation 2.**

This can be illustrated simply by figure 15.

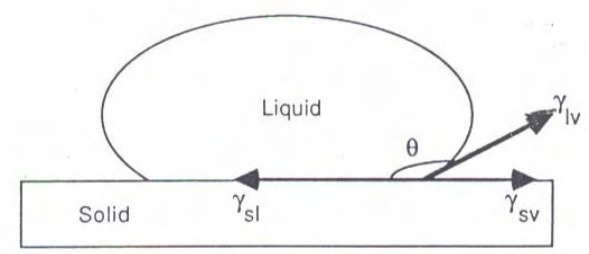


**Figure 15. Sketch of a wetting process showing surface tensions and the contact angle**

The occurence of surface tension on the surfaces of two different phases can be explained as follows qualitatively. The molecules at or near the surface are attracted by their neighbors in the direction inwards and parallel to the surface. However, this force is not balanced by a corresponding force outwards because of the different nature of the molecules of the two phases. This means that work has to be done to bring a molecule from the bulk of the phase to the surface and this additional energy governed by the molecules at the surface can be expressed as amount of energy per unit area [20]. This can also be illustrated by figure 16.

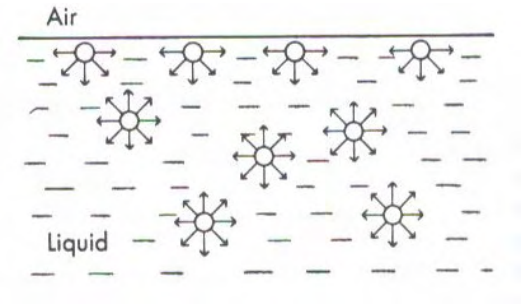


**Figure 16. Figure illustrating the attractive forces between molecules at the surface and in the interior of the liquid, which causes surface tension**

### 2.4.1 Types of Wetting

There are three types of wetting in general. These are:

1. Spreading Wetting
2. Adhesional Wetting
3. Immersional Wetting

To this study, spreading and immersional wetting is relevant. In spreading wetting, a liquid already in contact with the solid spreads to increase the solid liquid and liquid gas interfacial areas and decrease the solid gas interfacial areas. Thus, Young's equation can be derived from the thermodynamical equilibrium of the system easily. In immersional wetting, the solid which is not in contact with the liquid originally is immersed into the liquid completely. The area of the liquid gas interface therefore remains unchanged. The free energy change for immersion of a solid into a liquid is given by:

$$\Delta G_i = \gamma_{SL} - \gamma_{SG}$$

$$= - \gamma_{LG} \cos \theta$$

**Equation 3.**

So, if $\gamma_{SG} > \gamma_{SL}$, then $\theta < 90$ and immersional wetting is spontaneous. But if $\gamma_{SG} < \gamma_{SL}$, then $\theta > 90$ and work must be done to immerse the solid into liquid. In the case of immersional wetting, a decrease in $\gamma_{SL}$ or an increase in $\gamma_{SG}$ will decrease the contact angle, thus improves wetting. A change in $\gamma_{LG}$ will have an effect on the contact angle $\theta$ but immersional wetting is not affected. Capillary rise and pressure infiltration of a liquid metal into a solid preform are two practical examples of immersional wetting but related to this study, when a solid is immersed into liquid, immersional wetting also occurs and all the calculations above will be relevant.

If adhesional wetting is considered, where the solid gas interface area decreases which is the opposite to the case of spreading wetting, the work of adhesion is given by the Dupre equation as follows:

$$W_{AD} = \gamma_{SG} + \gamma_{LG} - \gamma_{SL}$$

**Equation 4.**

The work of adhesion is the work required to separate a unit area of the solid liquid interface into two surfaces [22]. Work of adhesion can be calculated from a sessile drop experiment which is used to obtain the $\gamma_{LG}$ and $\theta$ after combining the Young's and Dupre equation and inserting these values into the equation. The Young-Dupre equation is given below:

$$W_{AD} = \gamma_{LG} ( 1 + \cos \theta )$$

**Equation 5.**

The relation of work of adhesion to wetting of ceramics by molten metals is described in the next section.

### 2.4.2 Wetting of ceramic particulates in the production of MMC's

Good wetting is a necessary condition for the generation of a satisfactory bond between the solid ceramic phase and the liquid metal matrix during the fabrication of MMC's. This fact led the researchers to develop better methods to measure the wettability of these systems. Although it is a certain fact that the wettabilities of ceramic particulates can not be measured by conventional methods, first these conventional methods will be described and later the approaches to measure the wettabilities of ceramic particulates with molten metals will be described. After that, factors influencing the wetting angle, such as addition of alloying elements, chemical reactions between the matrix and the reinforcement or oxygen partial pressure will be described. Also, the effect of parameters such as the free energy of formation of oxides of the wetting metal on the wetting behavior (or on $W_{AD}$) will be discussed presenting a model which describes the interface between the solid ceramic and the liquid metal that influences wetting.

#### 2.4.2.1.Conventional Methods

##### 2.4.2.1.1 Sessile drop method

This method is the most easy and widely used method in determining the contact angle. In this method, a liquid drop is placed on a flat ceramic surface and by using microscopy or photography, the contact angle is measured.

In an early study by Champion, Keene and Silwood, [23] contact angle of molten aluminum on alumina has been measured using the sessile drop technique. Measurements were made as a function of time and temperature over the temperature range from 800 to 1500°C. The behavior of molten aluminum on

$Al_2O_3$ has been studied by previous authors as quoted by reference 23. It was found that molten Aluminum wet polycrystalline alumina at a temperature of 1255°C. It was also found that there was significant differences of spreading behavior in the case of single crystal and polycrystal alumina where in the case of polycrystalline $Al_2O_3$, the drop attained a steady shape and the contact angle attained a steady value whereas in the case of sapphire, the drop was observed to spread and contract repeatedly. Another observation was that, above about 925°C, sapphire was partially dissolved in aluminum and even below this temperature there was still some attack. Also in the study of Champion et al., some reaction rings were observed on the single crystal samples which correlates with the same fact. Succesive photographs taken at intervals of of 2 sec of a sessile drop of Aluminum on single crystal ruby at 1350°C is given in figure 17. It can be seen that the drop spreads and contracts repeatedly. Also, to observe the difference between the spreading and contracting behavior of the drop in the cases polycrystalline Alumina and single crystal ruby, figure 18 is helpful which shows the variation of the diameter of the solid liquid interface with time at 1350°C.

Variation of contact angle of molten aluminum on single crystal sapphire with temperature up to 1150°C is given in figure 19. It can be seen that wetting occured above about 1050°C where $\theta = 90$. This means that $Al_2O_3$ is not wet by molten aluminum at the temperatures close to the melting point of aluminum. In an other study by Naidich [24] where the wetting of some nonmetallic materials by molten aluminum was investigated using the sessile drop method, it was also observed that molten aluminum did not wet sapphire at the temperatures close to the melting temperature of aluminum. In another study [25] the temperature dependence of the wetting angle $\theta$ of Aluminum on compositions of an $Al_2O_3$ $ZrO_2$ system is investigated and it can be seen from figure 3 of this reference that at 100% $Al_2O_3$, molten aluminum starts to wet $Al_2O_3$ at temperatures exceeding 1100°C under vacuum conditions. In this study, the time dependence of the wetting angle $\theta$ is also shown. It can be seen from figure 20 that after about 20 min at 1100C, molten aluminum begins to wet the $Al_2O_3$ $ZrO_2$ system. This increase is attributed to the

chemical reaction between the overheated aluminum and the refractory. It was established that $Al_2O_3$ might react with Aluminum at temperatures between 1000

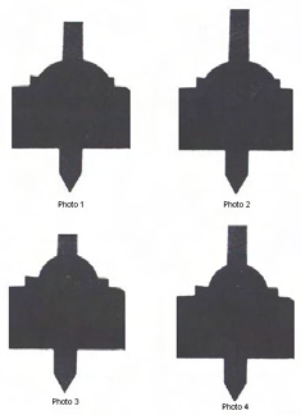


**Figure 17. Figure showing the repeated contracted and expansion of a liquid metal drop on a single crystal $Al_2O_3$ flat substrate (Photos are taken at two second time intervals)**

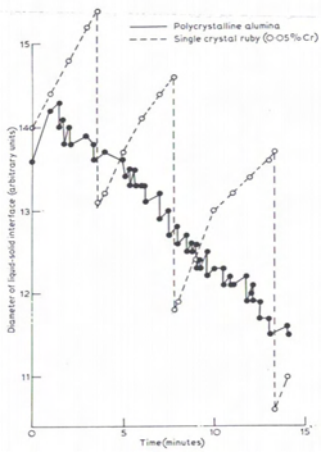


**Figure 18. Diagram illustrating the expansion and contraction of liquid metal drop on polycrystalline and single crystal alumina**

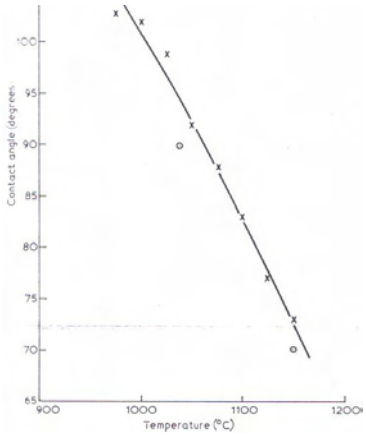


**Figure 19. Variation of contact angle θ with temperature of Al on $Al_2O_3$**

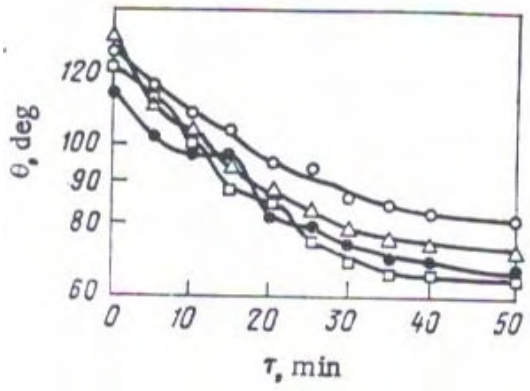


**Figure 20. Variation of contact angle θ with time of Al on $Al_2O_3$ (• represents 100% $Al_2O_3$)**

and 1100°C which results in the formation of monoxides which reduces the $\sigma_{sl}$ and therefore results in a decrease of the wetting angle.

The wettability of $TiB_2$ by aluminum melts is examined in reference 26. In this study, sessile drop method is applied to determine the wetting angle θ of aluminum

melt on $TiB_2$. At a temperature of 1000°C, $\theta = 114$ for this case. This means that $TiB_2$ is not wet by molten aluminum at this temperature and possibly near the

melting temperature of aluminum. In the same study, it is also indicated that the angle of contact is determined by the preferential migration of atoms which depends on the character of the chemical reactions between the materials at contact. $TiB_2$ is known to be non reacting with aluminum melt and so wetting of it is low by molten aluminum. In the table in this study, it can be seen that in the case of transport of elements from the refractory compound to the melt, wetting is not observed but in other cases wetting angle is lower than 90° for most cases. It is also said that rise in temperature activates the diffusion of elements from the melt to the compound. It can not be ruled that the oxide film on the melt becomes less firm under these conditions, this would also improve wetting by intensifying the transport of elements from the melt to the refractory compound. It is concluded that the wetting of a hard surface by a molten metal may be influenced by changing temperature and introducing one of the materials additions which affect the migration of atoms in a certain direction.

As a final for this part, the temperature dependence of the wetting angle of molten aluminum on $Al_2O_3$ which is obtained by different investigators is given in figure 1 of reference 27. The results obtained show significant differences especially at temperatures below 1000°C which might be due to the different experimental conditions of the various investigations.

#### 2.4.2.1.2 Capillary Rise Method

Capillary rise method is may be the most effective method in measuring wetting angle and $\gamma_{lv}$. A sketch of a capillary rise is given in figure 21 [21]. Since the measurements do not involve a disturbance of the surface, slow time effects can be followed. The way for calculating $\gamma_{lv}$ is given below:

**$\gamma_{lv} = r\ h\ \Delta\rho\ g\ /\ 2\cos\theta$**

**$\Delta\rho$ = Density of liquid – density of vapor**

**Equation 6.**

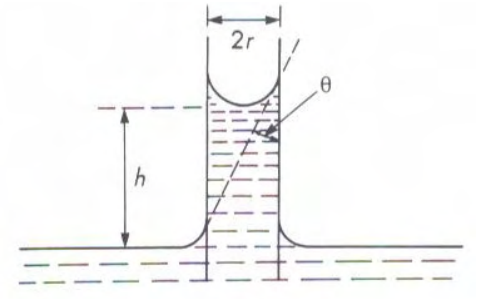


**Figure 21. Sketch illustrating capillary rise of a liquid**

In a study by Oh, et al. [28] the capillary rise equation was modified in order to measure the wettability of ceramic particulates by molten aluminum. According to them, the equilibrium of the liquid column in a porous solid preform requires a capillary pressure $P_c$ of;

**$P_c = 2\ \gamma_{lv}\ \cos\theta\ /\ rh$**

**$r_h$ = hydraulic radius = Volume of liquid column in capillary / area of wetted surface of capillary**

**Equation 7.**

In the case of a compacted powder, $r_h$ is as follows:

$$r_h = D\,w / 6\lambda\,(1 - w)$$

**D = Average diameter of ceramic particulate**

**w = Void fraction of powder compact**

**$\lambda$ = Geometry factor depending on the geometry of particulate and capilary channel**

**Equation 8.**

This formula has some drawbacks. First of all, it involves the wetting angle $\theta$ which is not always defined and the geometry factor $\lambda$ which may be hard to determine. Anyway, in their experiment they extrapolated penetration distance vs pressure curves back to zero penetration and obtained the treshold pressure. This gives a quantitative measure of wettability which is often needed by investigators in the case of wetting of ceramic particulates.

#### 2.4.2.1.3 Multiphase Equilibrium

Multiphase equilibrium method is used for measuring surface energies of solids and it is considered to be the most reliable method for this purpose. Another succesful approach is the zero creep technique. Despite the success of these methods, it is not possible to estimate the solid liquid surface energy accurately. This is due to the insufficient data on the solid vapor surface energy, $\gamma_{sv}$. As quoted by reference 29, Bruce [30] calculated the surface energy of oxides and carbides from the crystal structure, atomic bond energy and heat of sublimation of these. Nevertheless, using appropriate equations and data, the solid liquid interfacial energy and work of immersion can be calculated.

### 2.4.3 Issues of Wetting in Ceramic Particulate Reinforced Metals

If we now turn to casting processes where the ceramic is added to the liquid metal in powder form, the analysis becomes relatively simpler as the geometry of the problem is well defined if the interaction between particles engulfed is neglected. Then, the problem is of one particle at the surface between a liquid and gas. From equilibrium configurations, it is concluded that for engulfment of a smooth particle, an energy barrier must be overcomed even if the contact angle is less than zero. This is illustrated in figure 22 in the idealised case of the engulfment of a cubic particle with one face horizontal. For the last face to be wetted, the interface between the particle and the gas must be replaced with two interfaces. From the Young equation then, force must be applied on the reinforcement to produce the composite. In the case of real systems, the very last portion of a smooth particle is always horizontal, so the same conclusion is obtained. The usual method for producing composites in this case involves the use of motion in the metal in which uses viscous drag to pull them into the melt. Some modelling work was done on the application of viscous drag to pull the reinforcement in the metal [8] but there are limiting cases for these models because of the cuspidal points present on the surface of the reinforcing particles for which the wetting angle $\theta$ is not defined. Also the oxide layer is thicker than it is in the infiltration process which plays a significant role in wetting. Nevertheless, in figures 23 and 24, the effect of particle

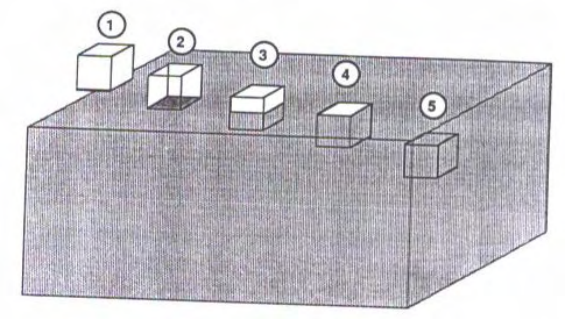


**Figure 22. Sketch showing the immersion of a cube into liquid. From step 1 into two, immersion is spontaneous irrespective of the wetting angle, however, from step 4 into five, it is energetically unfavourable regardless of the wetting angle**

size and and contact angle on the fluid flow velocity required for incorporation is given. As quoted by [11] particle size effect is also shown by Stefanescu et al., who measured the centrifugal force required to immerse particles in molten aluminum. When the particle size increases, a sudden decrease in the centrifugal force required to immerse particles is observed at the same particle radius of two oxide particles of different density. This decrease was attributed to the fact that the diameter of the particles exceeded the thickness of the oxide layer. Particles are also found to agglomerate at the metal surface before incorporating to the melt and this makes the problem more complex. In spite of all these limitations, it is indicated that it is possible to correlate wetting data with processing parameters and these indicate that finer particles are harder to incorporate which is consistent with this fact.

The measurement of wettability by the sessile drop method is discussed in the previous section. A general conclusion is that the experiments made by this technique are reliable, although it is also indicated before that measurements of various investigators differ from each other. This is because these data depend on several complicating factors. These are:

1. With several metals including aluminum, the presence of an oxide layer on the metal prevents it to contact the substrate and therefore influences

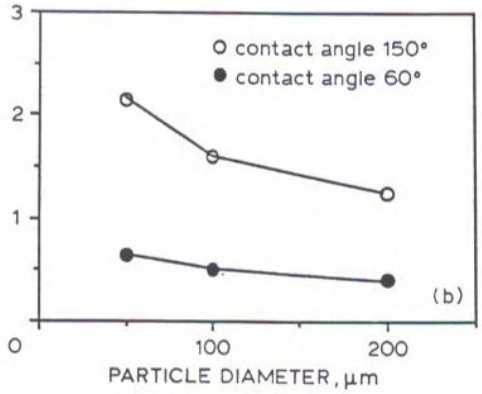


**Figure 23. Particle diameter vs minimum fluid velocity required to incorporate particles into melt**

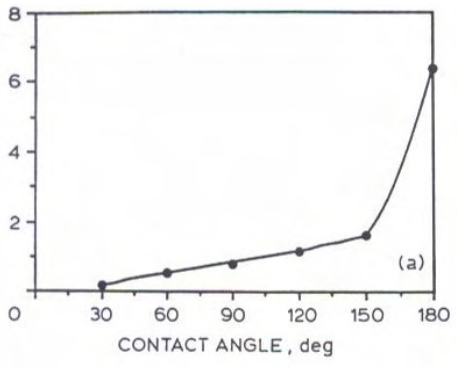


**Figure 24. Contact angle vs minimum fluid velocity required to incorporate particles into melt (for particles of 100μm diameter**

wetting. The presence of abrubt wetting non wetting transition temperatures which is also shown in figure 25 depends on this fact as well as on the fact that alloying aditions or temperature changes affect the oxide layer covering the melt.

2. Wetting angle data is often time dependent. This phenomenon is thought to be observed because of the chemical reactions occuring at the interface between the metal and the substrate and the necessity for the metal to break through its oxide layer to maintain contact with the substrate.

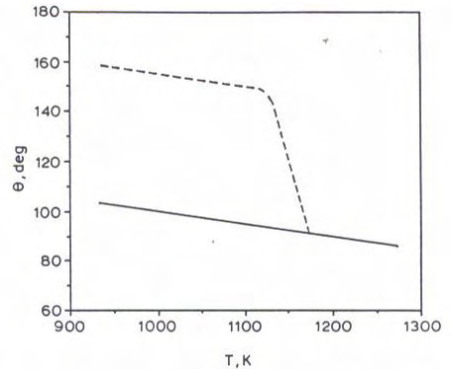


**Figure 25. Variation of wetting angle by temperature (— Oxygen partial pressure $10^{-15}$ Mpa, ---- Oxygen partial pressure > $10^{-6}$ Mpa). The abrupt change in the curve above is due to the evaporation of the oxide layer at around 1150K.**

Thus, the dependence of wetting angle data obtained by sessile drop method on these phenomena invalidates the direct application of sessile drop wetting angles to metal matrix composite solidification processes as the velocity of the three phase contact line is much higher than they are in the sessile drop experiment, as the oxide layer is disrupted by the reinforcement as it combines with the metal or as there is microscopic roughness and chemical inhomogeneity on the surface of many reinforcements. Mortensen [31] also indicates that the sessile drop experiment only replicates poorly the wetting conditions in metal matrix composites fabrication. He adds that even if θ is measured, its correlation with processing parameters is not easy to explain. In the case of stirring a particulate reinforcement into a molten metal, the correlation between particle size, stirring velocity, wetting angle and particle engulfment kinetics is not simple as shown by Illegbusy and Szekely [8]. In this study, the situation of a single particle being immersed into the melt is modelled together with the forces acting upon the particle which is shown in figure 26. The forces acting upon the particle are the buoyancy force on the immersed part, gravity on the whole particle, surface tension at the solid liquid interface in the vertical direction and drag force on the particle due to fluid motion. In figure 27, which shows the resultant forces for a given size particle as a function of the contact angle for different stages of immersion characterized by the semiepical angle w which is shown in figure 26, it can be seen that the contact angle ( influences engulfment to a great extent but the semiepical angle also influences engulfment. Another figure from this study, figure 28 illustrates the effect of particle diameter on the resultant force where it can be seen that when the particle size is smaller the resultant force is larger. It is indicated that this is consistent with the expectations because the surface forces inversely vary with the particle diameter. In this study, it is also indicated that the critical melt velocity by electromagnetic agitation increases when the contact angle is high which is illustrated by figure 29. Figure 30 shows the combined effect of the particle diameter and contact angle on the minimum (critical) velocity required to incorporate particles in the melt. It can be seen that especially when the contact angle is high, it is difficult to incorporate small particles in the melt. The conclusion that can be obtained from all of these is that, when the particle is not wetted by the liquid metal, engulfment is very difficult and would require

unrealistic melt velocities provided by electromagnetic agitation. This can be seen from figure 31, where the realistic range of minimum induction current is for a contact angle of 20 – 30(. Thus, one needs other forces i.e. mechanical stirring, to incorporate particles that are not wet by the liquid metal. As a final explanation, these limitations of sessile drop experiments to characterize wetting led the development of alternative measuring methods such as the one described in the section capillary rise in this study.

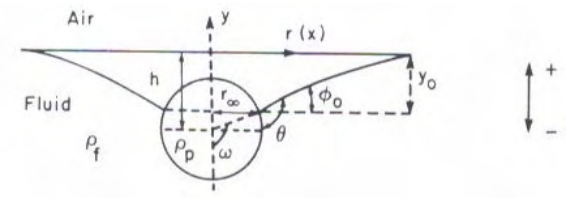


**Figure 26. A sketch of the intermediate stage of immersion of a spherical particle into liquid metal**

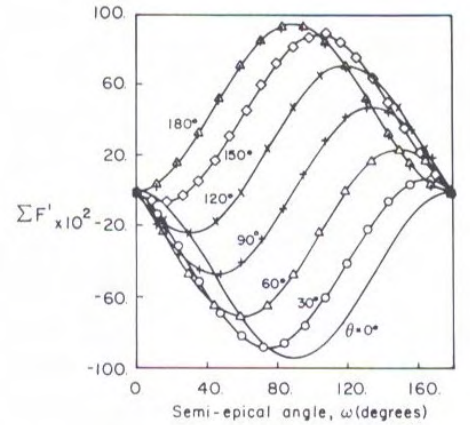


**Figure 27. Sum of forces acting on a 200µm particle at various stages of immersion (w) as a function of the contact angle**

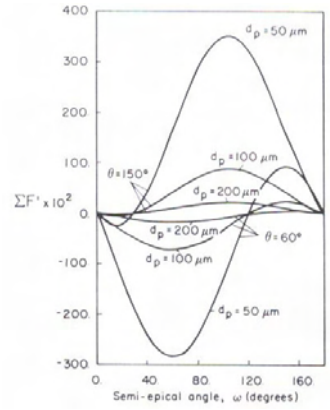


**Figure 28. Effect of particle size on sum of forces acting on a particle at various stages of immersion (w)**

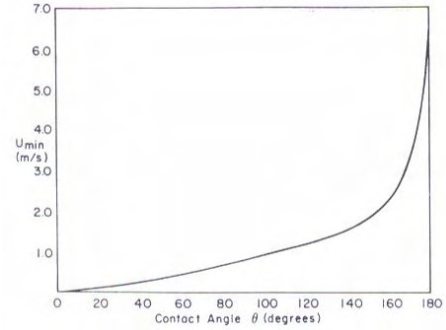


**Figure 29. Minimum required characteristic velocity for different contact angles**

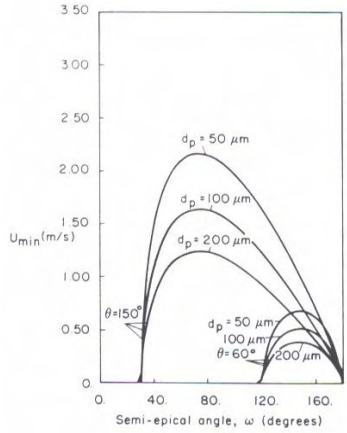


**Figure 30. Semiepical angle vs minimum required characteristic velocity with particle size and contact angle as parameters**

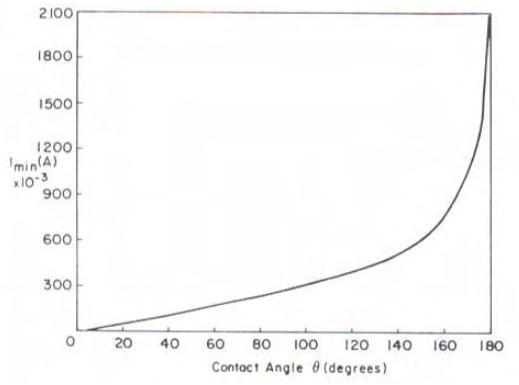


**Figure 31. Contact angle vs minimum induction current required for incorporation**

On the basis of wetting angle data, spontaneous wetting of a reinforcement by a molten metal is found to be promoted by some reactivity of the metal with the substrate or by reduction of the tenacity of the oxide layer on metals which have tenacity to oxidize, such as aluminum. Depending on these observations, much work has been done to find means of enhancing the poor wetting of ceramics by molten metals. Most of this work has been classified into two categories: Alloying additions and reinforcement coating. In addition to these, the atmosphere of the system is designed such that $\gamma SG$ of the reinforcement increases which promotes wetting and heat treatment of particles such as alumina, graphite and silicon carbide improved their ease of incorporation into molten aluminum which is attributed to the desorption of the gaseous species from the reinforcement surface during heat treatment.

Effective alloying additions fall into two categories:

1. Additions that promote reactions between the reinforcement and the matrix
2. Additions to aluminum that do not promote reactions with the matrix but modify the characteristics of the oxide layer on the metal surface

Most research on the structure of surfaces and interfaces is for relatively pure metals and reinforcements. When the metal is alloyed, both its surface tension and

the metal reinforcement interfacial energy is affected especially when alloying additions tend to segregate at the interface. It is known that Mg addition to aluminum lowers the solid liquid interfacial energy between the melt and alumina particulate reinforcement. By this way, it is observed that Mg improves wetting between liquid aluminum and alumina in sessile drop experiments, in some stirring processes and in the LANXIDE™ process [32].

The effect of oxygen partial pressure on the wetting behavior in the system Al Al2O3 has been investigated by Hausner [27]. In figure 32 the dependence of the wetting angle on the oxygen partial pressure is plotted and as a result it is indicated that at very low oxygen partial pressures such as 10 –49 bar at 700ºC, wetting angles as low as 90º can be obtained.

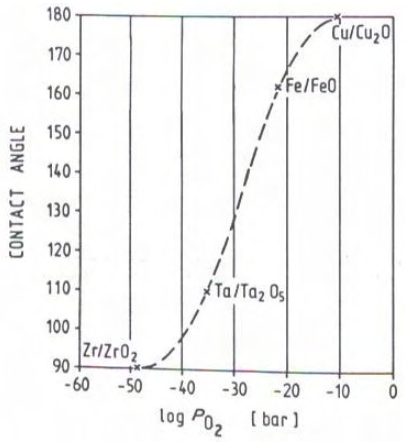


**Figure 32. Oxygen partial pressure vs contact angle of liquid Aluminum on $Al_2O_3$**

Finally, adhesion of metals, especially aluminum on Al2O3 is investigated by McDonald and Eberhart [22]. They propose a model for the interface between aluminum and Al2O3 and based on this model they attempt to calculate work of adhesion theoretically. In order to have an idea about the interface type and bonding, figure 33 is helpful. According to this proposed model, there are two types of interaction between the aluminum metal and Al2O3, namely Van der Waals and chemical interactions. These two types of bonding takes place between

oxide ions and the metal atoms and in one case (where the metal atom on A site) bonding is chemical and in the other case (where the metal atom is on B site) Van der Waals. They also point that wetting of Al2O3 and other substrates by several metals including aluminum increases with increasing negative values of the free energy formation of oxides of these metals which is also investigated by Humenik and Hingery as quoted by McDonald and Eberhart [33].

.

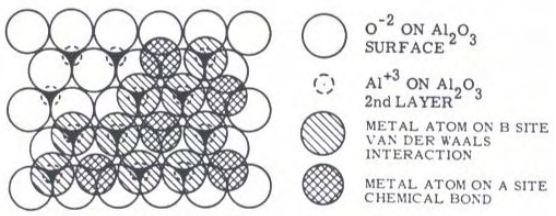


**Figure 33. <0001> surface of sapphire showing sites of chemical interaction (A) and Van Der Waals interaction (B)**

### 2.5 Solidification Of Metal Matrix Composites

Solidification of metal matrix composites is important as it determines in large extent the final composite microstructure. For this reason, a better understanding of this phenomena is necessary at the beginning. Direct application of rules governing the solidification of unreinforced matrices is not always possible as the reinforcement usually modifies the solidification of the matrix. In the following explanation, it is assumed that the reinforcement does not go into reaction with the matrix because very little fundamental work has been done for the opposite case.

The solid reinforcement can reduce the grain size of the matrix if it catalyses heterogeneous nucleation of the primary metal phase. This rarely seems to occur with aluminum since grain sizes far in excess of reinforcement diameter is observed in many cases where it is reinforced with alumina, carbon and silicon carbide fibers or particles. However, when the reinforcement provides appropriate sites for the nucleation of the matrix, grain refinement might occur. An example is the case of TiC reinforced aluminum. Some grain refinement was also found in Ti-

51.5 Al-1.4 Mn reinforced with less than 10 vol% $TiB_2$ particles as quoted by reference 11. Grain refinement of the matrix may occur because of the exchange of heat between reinforcement and matrix during infiltration. When the reinforcement does not promote nucleation of the primary metal phase by catalysis or heat transfer, the grain size of the composite is greater than of the identical casting of the unreinforced alloy. This is because the reinforcement hinders the convection of the liquid metal. Many mechanisms responsible for the formation of fine equiaxed dendritic structures in castings depend on fluid flow. Because of this, if there is significant convection during solidification of a similar unreinforced casting and matrix nucleation is slow, an increased propensity for columnar dendritic solidification in composites is expected.

The growth of the solid metal is investigated under two different conditions, where the reinforcing phase is stationery or it is mobile. The reinforcement is generally stationary in the case where it is in the form of fibers and it is usually mobile when it is in the form of fine particles. The first case will be omitted and the second case will be focused as it is relevant to the subject of this study. When a moving solid liquid interface approaches a mobile particle suspended in the liquid metal, the particle can either be engulfed or rejected by the interface. If particles are engulfed, there will be little redistribution of them in the matrix so the resulting particle size distribution will be as uniform as it was in the liquid state. On the other hand, if particles are pushed by the solidification front, they will be redistributed finally segregating in the last pools of the liquid metal solidifying.

The parameters affecting particle engulfment or rejection can be summarized as particle radius, viscosity of the liquid, thermal conductivity ratio of the particle and the liquid, surface energy among particle, liquid and solid, particle shape and aggregation convection level in the liquid, density of the liquid and the particle. Additional variables can also be considered which are liquid solid interface shape, volume fraction of the particles at the interface and temperature gradient ahead of the interface.

Referring to reference 11, the first systematic work on particle pushing is by Uhlmann et al. They found that in some systems a critical velocity, $V_C$, existed below which the particles were pushed and above which they were captured. After that, a series of experiments were conducted by different investigators. As indicated by reference 11 again, Cisse and Boiling found that regardless of the particle type, $V_C$ decreased when particle size increased and when the liquid viscosity increased. Zubko et al. examined experimentally the effect of thermal conductivities of the particle and the matrix on particle engulfment as quoted by reference 11. It was found that when the thermal conductivity of the particle was higher than that of the liquid, particles were engulfed and otherwise rejected.

After all these studies, it is established that there are two theoretical approaches to the study of the particle behavior at the solid liquid interface, thermodynamic and kinetic approaches. The thermodynamic aspect has been studied by Omenyi and Neumann [34]. In their study, they stated that if the rate of solidification is low and and the solid melt interface is smooth, thermodynamic effects predominate. In figure 34 the thermodynamics of the engulfment of a particle is illustrated. The condition assumes that if the net free energy change during particle engulfment is less than zero, particle is engulfed, otherwise it is rejected.

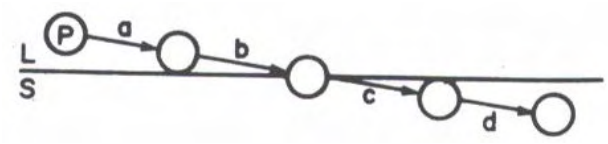


**Figure 34. Sketch showing the thermodynamics of the engulfment of a sphere of unit surface area**

Omenyi and Nemann also formulated the critical velocity by curve fitting of the experimental data as:

$$V_c\, r^n = \text{constant}$$

**r: Particle radius**
**n: a constant ranging from 0.28 to 0.90**

**Equation 9.**

The kinetic approach is based on the idea that as long as a finite layer of liquid layer exists between the particle and the solid, the particle will not be engulfed.

The influence of the temperature gradient G on the critical velocity is that the critical velocity increases with increasing G.

The effect of fluid convection in the melt on particle pushing is investigated for metallic systems [11]. When the interface was planar the particles were uniformly distributed in the solid, indicating that the particles were not pushed by the planar interface. When the interface was cellular, the particles segregated to the cell boundaries. These studies indicate that when there is convection in the melt, and if the solid liquid interface is non planar, convective flow can take the particles away from the cell or dendrite tips, resulting in intercellular or interdendritic segregation. In figure 35 [52] possible types of structures that can be formed during multidirectional solidification is presented.

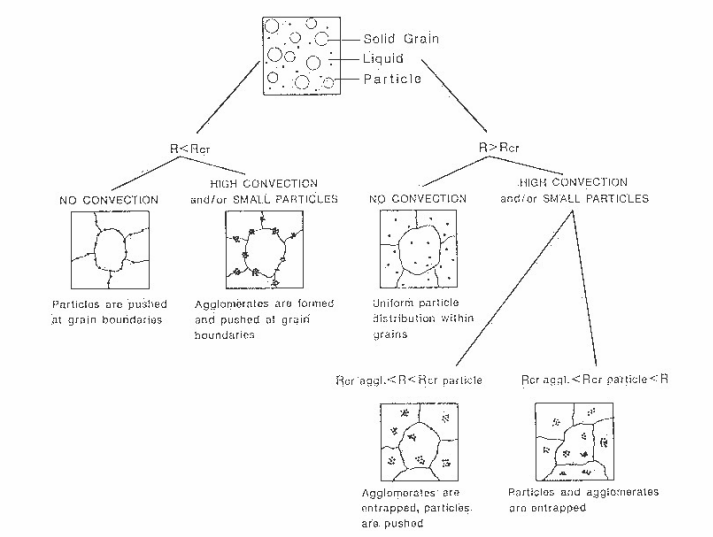


**Figure 35. Possible multidirectional solidification structures as a function of solidification rate, convection level and particle size**

In some directional solidification experiments with controlled temperature gradients, particle behavior was studied by examining the quenched solidification front. However in most other cases, particle behavior was inferred from the particle distribution in the resulting microstructure after solidification, by examining whether particles are located in the interdendritic regions or inside dendrite cells. This method is good when the dendrite arm spacing is greater than the particle size. However when the solidification rate is high and the dendrite arm spacing is less than the particle size, the microstructure does not indicate whether the particles are captured or mechanically locked between dendrite arms.

The wide range of experimental data leads to three conclusions:

1. Some particle matrix combinations exist where the particles are captured in all growth conditions. In these systems, the net free energy change is negative, i.e. particle solid interfacial energy is lower than the particle liquid interfacial energy. In metal matrix composites, graphite or SiC

particles in eutectic and hypereutectic Al-Si alloys are examples of this category.

2. There are some particle matrix combinations where the particles are rejected at a growth velocity lower than a critical velocity, $V_c$ and engulfed at higher velocities. When the solid liquid interface is planar, $V_c$ is given by the formula indicated above and it is dependent on the interface chemistry, particle size, liquid viscosity, temperature gradient, thermal conductivities of particle and matrix and solute content.
3. There are particle matrix combinations where the particles are pushed at any growth conditions. Some examples are $Al_2O_3$, SiC, $TiB_2$ and $ZrB_2$ – Al – 3Mg. Most hypoeutectic Al alloy matrix composites tested with a nonplanar interface shape fall into this category.

## 2.6 Interfaces In Metal Matrix Composites

The inerface region in a composite is very important since it determines the final properties of the composite. Theoretically, interface is a bidimensional region where a discontinuity occurs in one or more material parameters. However in practice there is always some volume present within the interface region over which a gradual transition in material parameters is present. The importance of the interface region in composites is due to two main reasons:

1. The interface contains a very large area in composites
2. In general, reinforcement and the matrix form a system which is not in thermodynamic equilibrium.

Among the important discontinuities in the interface region are elastic moduli, chemical potential and CTE. The discontinuity in chemical potential leads to chemical interaction which results in an interdiffusional zone or chemical compound formation at the interface. The discontinuity in the thermal expansion coefficient means that the composite will be in equilibrium only at the temperature

where the matrix and the reinforcement were brought into contact. At other temperatures, stress fields will be present due to the difference in the CTE of the reinforcement and the matrix.

Some bonding must exist between the ceramic reinforcement and the metal matrix. In this case, load transfer from the matrix to the reinforcement occurs. The applied load will be transferred from the matrix to the reinforcement via a well bonded interface. The bonding at the interface might be either chemical or physical. Chemical bond is stronger than physical bond but under perfect wetting conditions, physical bonds such as Van Der Waals bonds might be enough to produce a well bonded interface [53]. A controlled interfacial reaction between the matrix and the reinforcement can provide good adhesion. A diffusion barrier coating between the reinforcement and the matrix is frequently employed to control the extent of a chemical reaction. So it is important to understand the thermodynamic, kinetic, mechanical and microstructural aspects of a metal ceramic interface in order to use that information to optimize the processing to get useful characteristics of interfaces in MMC's.

Most MMC systems are not in thermodynamic equilibrium, there is a chemical potential gradient accross the interface. This means that in favorable kinetic conditions, meaning a high enough temperature or long enough time, diffusion and chemical reaction will occur between the matrix and the reinforcement. The interface formed by such a reaction generally have different characteristics than either of the components.

Ceramic metal interfaces are generally formed at high temperatures as diffusion and chemical reaction kinetics are faster at high temperatures. So, various processing parameters such as time, temperature and pressure combined with the thermodynamic, thermal and the kinetic data can be used to obtain optimum interface characteristics in metal matrix composites.

### 2.6.1 Interfacial Reactions Between Alumina Particles and Aluminum alloys

Most of the ceramic reinforcements are unstable at high temperatures and long processing times so they undergo reactions with the alloying phase in the matrix. These reactions produce chemical reaction products at the interface which might be beneficial or undesirable for the composite strengthening. These reactions often remove a desired phase from the composite and form undesirable compounds.

In the case of an alumina particulate reinforced aluminum composites, aluminum oxide which is stable in aluminum matrix becomes unstable in the presence of magnesium and forms either $MgAl_2O_4$ spinels for Mg contents between 1 wt% and 4wt% or MgO for Mg contents greater than 4 wt% [35]. Spinel formation can also proceed in the solid state as $Al_2O_3$ remains unstable below the solidus line but this reaction is favored at high temperatures so practically the kinetics and extent of the reaction has to be considered. Kinetics of the spinel forming reaction is studied by McLeod and Gabryel [36]. They first indicate that the growth of spinel consumes the magnesium required for age hardening and increases the viscosity of the melt and effects the castability of the material. On $Al_2O_3$, MgO and $MgAl_2O_4$ form according to the reactions;

$$\mathbf{3\,\underline{Mg} + Al_2O_3 = 2\,\underline{Al} + 3\,MgO}$$

$$\mathbf{3\,\underline{Mg} + 4\,Al_2O_3 = 2\,\underline{Al} + 3\,MgAl_2O_4}$$

Using free energy formation data and activity coefficient data for the Al Mg binary, the Mg concentration in equilibrium with these reactions for liquid alloys can be calculated. The result is shown in the figure 36 from the same study. It is also apparent from the figure that $Al_2O_3$ is not stable in the solid state with Al Mg alloys. They finally plotted Mg concentration versus time for different temperatures and found that the growth of spinel on $Al_2O_3$ particles in Mg containing Al alloys follow a decelatory growth mechanism. In figure 37 change in

the rate of Mg content with respect to different initial magnesium contents is also shown which is taken from another study [35].

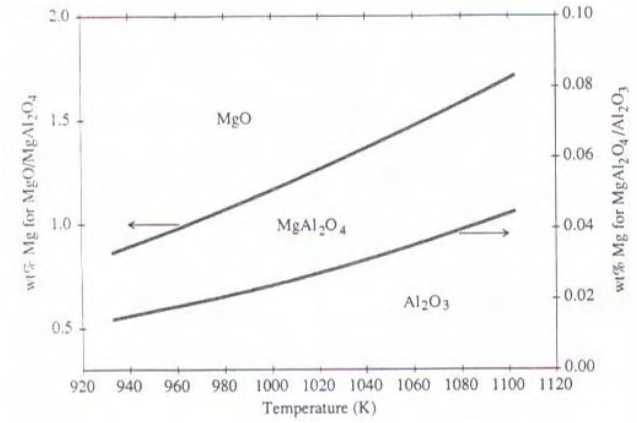


.

**Figure 36. Thermodynamical stability diagram of al Mg oxides in liquid Al Mg alloys**

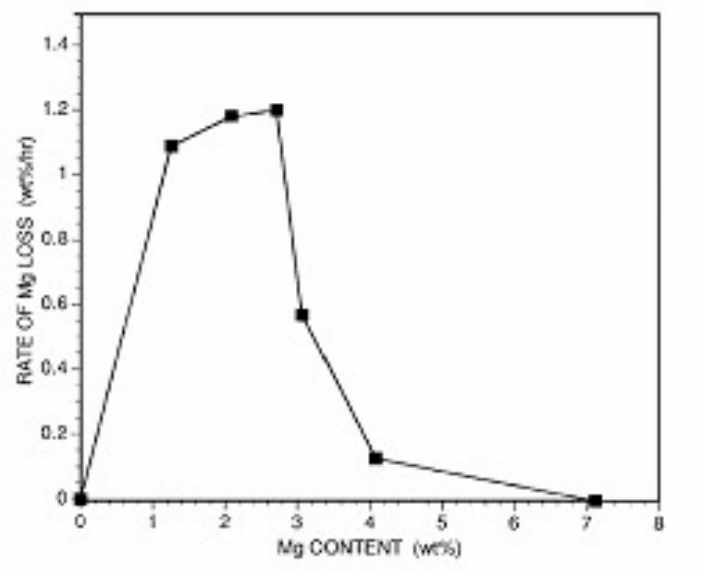


**Figure 37. Change in the rate of Mg content with respect to different initial Mg contents**

On the other hand, Lee and Subramanian [37] studied the interfacial characteristics of the interface $Al_2O_3$ and Al. They detected by X-ray diffraction and SEM analysis that nearly all of the $Al_2O_3$ particles were covered with $MgAl_2O_4$ spinels. It is noted furthermore that the inner surface contour of $Al_2O_3$ which surrounds the $MgAl_2O_4$ crystals matches the outer contour of the $MgAl_2O_4$ crystals. This indicates that the bonding between $Al_2O_3$ and $MgAl_2O_4$ crystals is strong. It is known that cracking in particulate reinforced metals can occur either by particulate cracking or interfacial debonding. They noted that as nearly all of the $Al_2O_3$ particles are covered with a 1 mm thick $MgAl_2O_4$ layer, interfacial debonding can occur either at the $Al_2O_3$ / $MgAl_2O_4$ phase boundary, at the $MgAl_2O_4$ / Al phase boundary or at the $MgAl_2O_4$ layer itself by fracturing single crystals. Among these, the first one has never been observed but second one is frequently observed. The third one is less frequently observed and this also confirms that $Al_2O_3$ and $MgAl_2O_4$ has a strong interfacial bond. This can be illustrated by figure 38. It is also noted that jagged edges of $Al_2O_3$ particles produced as a result of severe interfacial reaction might cause stress concentration and help particulate cracking.

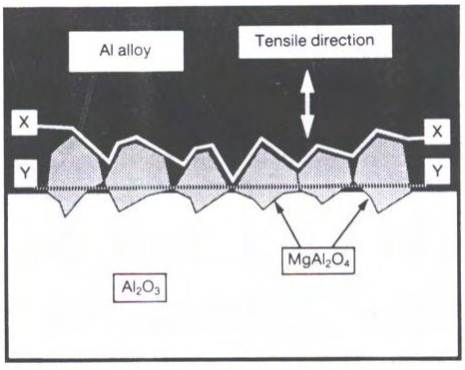


**Figure 38. Schematic illustration of interfacial debonding. Line XX represents debonding along the $MgAl_2O_4$ Al boundary. Line YY represents represents debonding along the $MgAl_2O_4$ itself.**

The strength and ductility of $Al_2O_3$ Al composites are lower than that of SiC Al composites at the same volume fraction of reinforcement although mechanical properties of $Al_2O_3$ and SiC are similar. In SiC Al composites, particulate cracking is found to be more predominant than interfacial debonding. However, significant interfacial debonding occurs in addition to particulate cracking in $Al_2O_3$ Al composites. In the case of interfacial debonding, load transfer form the matrix to the reinforcement becomes less effective and this can be the reason why $Al_2O_3$ Al composites have lower strength and ductility than SiC Al composites at the same volume fraction of reinforcement.

According to some investigators, formation of a $MgAl_2O_4$ spinel layer on the $Al_2O_3$ particles increases the strength of the composite whereas some others indicate that this formation of spinel decreases the strength of the composite. According to reference 35, above 4 wt% Mg, Mg and $Al_2O_3$ form MgO and between 1 and 4 wt% Mg, they form spinel. So, if one wants to control the extent of spinel formation, one can form a MgO barrier layer on $Al_2O_3$ particles using first Mg content of above 4 wt%. Then desired content of Mg can be obtained by adding more aluminium to the melt. Other solutions are possible such as alloying the matrix with an element that segregates at the interface and inhibits the spinel growth such as Strontium as quoted by reference 35.

Unlike $Al_2O_3$, $TiB_2$ is unreactive to most matrix alloys including Al Mg alloys.

**2.7 Porosity**

Porosity in aluminum alloy castings occur from two reasons:

1. Rejection of the dissolved gas from the liquid metal due to the decreasing solubility of it in lower temperatures during solidification

2. Inability of the liquid metal to feed through the interdendritic regions to compensate for the volume shrinkage during solidification

Hydrogen is the only gas that dissolves in liquid aluminum and the dramatic decrease in its solubility at solidification leads to the formation of porosity. Porosity results in reduced mechanical properties and corrosion resistance so its control is very important.

The formation of porosity can be controlled by adjusting hydrogen concentration and by other factors such as grain refining and inclusion content. In the case of the addition of grain refiners, as these grain refiners act as heterogeneous nucleation sites for the primary metal or alloy dendrites, a uniform, equiaxed grain structure is formed. This leads to a finer dispersion of pores and even a reduction in the amount of porosity.

Porosity formation in Al Cu Si alloys is studied metallographically by Roy et al [38]. They studied the effect of grain refining and alloying additions on porosity. In the case of grain refining, the addition of $TiB_2$ as a grain refiner led to a reduction in pore size and increase in pore density (number of pores / $cm^2$). Alloying with Mg introduced an interesting effect by decreasing the amount of porosity without influencing the pore size or shape. The reason for this could not be fully understood yet. The combined effect of Mg and grain refiner $TiB_2$ is more pronounced. It must be noticed that these conclusions are derived by examining unreinforced alloys. In the case of reinforced alloys, porosity tends to show an increase compared to the unreinforced counterparts [39].

Other parameters that influence porosity are called thermal parameters which are solidification time and solidus velocity. For a given hydrogen level, an increase in the solidifcation time increases percent porosity, pore length and pore area. The

reason for this depends on the fact that growth of porosity is diffusion controlled. All parameters also increase with an increase in the solidus velocity. This behavior can be explained by two nonexclusive phenomena: Reduction of the metal pressure due to the decrease of the permeability of the liquid solid zone and expansion of pores in isolated liquid pockets during the volumetric contraction of the last liquid to solidify. These isolated liquid pockets are reffered to as microhot spots.

### 2.8 Particle Size and Shape

The degree of strengthening in particulate reinforced metal matrix composites is closely related to particle distribution and shape. Particle distribution can be specified by volume fraction of particle, average diameter of particle and mean interparticle spacing [40]. These factors are interrelated so one of them can not be changed without affecting the others. As an example, for a given volume fraction, reducing the particle size decreases the mean interparticle spacing. For a given size, mean interparticle spacing decreases with an increase in the volume fraction.

There are several ways which fine particles act as a barrier to dislocations. One of them related to particulate reinforced metals is that, particles resist to be cut by dislocations as they are hard and the dislocations are forced to bypass them. This situation increases the strength of the composite.

When particle size is smaller at the same volume percent reinforcement, strength of the composite increases. Experiment and theory justifies this effect. An explanation of this can be that the strength distribution of a ceramic particulate population qualitatively follows Weibull's weakest link effect. A statistical theory of brittle fracture assumes that if there is no interaction between cracks in a rigid body, the strength of the composite is determined by the element with the longest crack. Weibull statistical distribution is appropriate in representing this situation [41] relating the fracture strength to the number of cracks. If this is adapted to particulate reinforced composites, large particles are more likely to contain critically sized flaws, which severely reduces the strength of the composite.

The importance of particle shape arises from the fact that matrix stress and strain fields developed in response to external loads vary significantly with the geometry of the reinforcing phase. Experimental evidence indicates that voids nucleate preferentially at the sharp corners of ceramic reinforcements. These voids lead to the premature failure of composites. According to this, it is useful to use spherical reinforcements to reduce stress concentrations thus changing the stress and strain distribution throughout the composite. In an investigation by Song et al. [42] the difference in strength, ductility and fracture behavior of 6061 Al matrix $Al_2O_3$ reinforced composites reinforced with angular and spherical reinforcements is considered. In figure 39 which shows the true stress vs true strain plots for composites reinforced with angular and spherical shaped reinforcements, it is apparent that composites reinforced with angular particles exhibit high yield strength and lower elongation to failure, hence lower ductility. This is attributed to the observation of the fracture surface by SEM that unlike the spherical composite where failure occurs by matrix void nucleation and growth, angular composite fracture is due to particle fracture.

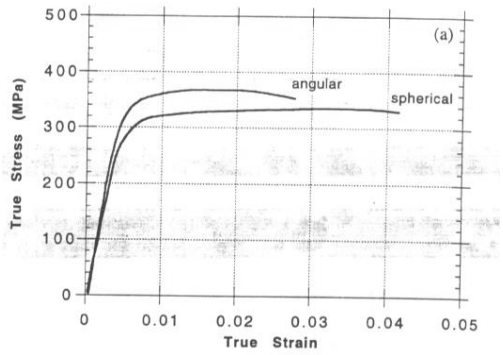


**Figure 39. True stress strain curve of spherical and angular particle reinforced composites**

In addition to these the spatial distribution of the particles is also important. In the work by Mummery et al. [43], it is indicated that when there are cluster of particles in the matrix, these cluster regions due to the high volume fraction of particles

locally, impose a much larger constraint on matrix deformation. Thus, void nucleation in clusters can occur at lower strains than elsewhere in the matrix.

Summarizing these, it is a fact that when the second phase particle is in the shape of rods or platelets, the strength can increase by an order of two compared to the case that particles are spherical. The strength of the composite where the particles are angularly shaped is higher than those where the particles are spherical but the ductility in this case is lower than the case where the reinforcement is spherical at the same volume fraction of reinforcement.

## 2.9 Strengthening Mechanisms in Particulate Reinforced Metal Matrix Composites

There are two approaches to predict mechanical properties of materials. These are the continuum approach and micro mechanistic approach. Continuum approach assumes that the properties can be described by global parameters. Micro mechanistic approach uses models built from a knowledge of the deformation processes at the atomistic level.

In this part, various strengthening mechanisms that are derived for particulate reinforced metal matrix composites using micro mechanistic approach will be discussed. Infact, most of these mechanisms are first derived for conventional particle containing alloys but in some extent they can be applied to particulate reinforced metals.

In a study by Miller and Humphreys [44], these mechanisms are discussed for particulate reinforced metals. The first mechanism is quench strengthening. The large difference in thermal expansion or CTE between the matrix metal and the particulate results in the generation of dislocations on quenching from the recrystallization or solution treatment temperature. The dislocation density generated on quenching is a function of reinforcement size, reinforcement volume

fraction and the product of the thermal mismatch and the temperature change. The strength can be given by an equation shown below:

$$\sigma_d = \alpha G b \rho^{1/2}$$

$$\rho = 12 \Delta T \Delta C F_v / b d$$

**$\sigma_d$ = Strength (0.2% offset yield strength)**

**$\alpha$ = A constant between 0.5 and 1**

**G = Materials shear modulus**

**b = burger's vector**

**$\rho$ = Dislocation density**

**d = Reinforcement size**

**$F_V$ = Reinforcement volume fraction**

**$\Delta C$ = Product of the thermal mismatch**

**$\Delta T$ = Temperature change**

**Equation 10**.

This analysis assumes that the dislocations are distributed uniformly and all dislocations generated contribute to strength. It is also indicated that this may not be true for a solution hardened matrix.

The second mechanism related also to the present work as well as quench strengthening is grain strengthening. In the presence of grain refiners, particles may act as nucleation sites for grains and grain sizes considerably finer than the grain size of unreinforced alloys might occur. This might contribute to the strength of the material formulated by the Hall – Petch equation given below:

$$\sigma_0 = \sigma_i + k\, D^{-1/2}$$

**$\sigma_0$ = Yield stress**

**$\sigma_i$ = The friction stress representing the overall resistance of the lattice to dislocation movement**

**k = The locking parameter which gives a measure of the relative hardening condition of the grain boundaries**

**D = Grain diameter**

**Equation 11.**

There are other mechanisms which are effective in certain situations in the case of particle reinforced metals such as Orowan strengthening, Sub structure strengthening and work hardening but these are not directly related to the present study. For example, Orowan strengthening occurs when the particle size is less than 1 μm and others occur during secondary processing routes such as heat treatment or work hardening. However, as quoted by reference 44, Humphrey's has also shown that these mechanisms can not be added linearly since the various mechanisms will interact with each other. Indeed, in this study, an attempt has been made to predict the yield strength of the composite by adding up the effect of the two mechanisms described above.

# CHAPTER III

## EXPERIMENTAL PROCEDURE

### 3.1 Introduction

First of all, ceramic product which consists of 29 wt% $TiB_2$ and 71 wt% $Al_2O_3$ was produced by a thermite reaction of reactants $TiO_2$, $B_2O_3$ and Al. The reaction product was in the form of a porous pellet and this pellet is characterized by SEM and EDS analysis to identify the two phases. Then, this powder was ground to fine powder size. The powder is characterized by X – Ray diffraction analysis to identify and verify if the correct phases are produced with no intermediate reaction products or unreacted reactants. After that, the powder was incorporated into liquid Al – 2%Mg alloy manually. The metal matrix composite was then cast by using pressure casting, when a $TiB_2$ - $Al_2O_3$ particulate reinforced aluminum composite is produced. By this method, four different castings were produced which include unreinforced matrix alloy, 3.54 vol% reinforced alloy and two samples of 5.84 vol% reinforced alloy, which are sample 1, sample 2, sample 3 and sample 4 respectively. The tensile strength and hardness of these castings were determined. After that, these samples were examined metallographically by optical microscope and SEM analysis and the results are discussed in chapter IV.

### 3.2 Materials Used In the Production of the Composites

The reactants of the thermite reaction were $TiO_2$ (rutile with purity > 99.5%), $B_2O_3$ (purity > 99.9%) and Al (purity > 99.9%). All the reactants were in fine powder size and were obtained from Merck Chemicals Company. $B_2O_3$ is known to convert to $H_3BO_3$ reacting with water. The $B_2O_3$ used in this experiment was tested to determine the amount of conversion by the following procedure: 10 grams of powder assumed to contain X grams of $B_2O_3$ and Y grams of $H_3BO_3$ (Boric Acid) was added into pure water and mixed to convert all of it into $H_3BO_3$. The conversion reaction is as follows:

$$B_2O_3 + 3H_2O = 2\ H_3BO_3$$

The solution was then dried slowly to obtain only solid $H_3BO_3$. The weight of this solid , W, measured as 11.74 grams should be given by;

$$W = 2 \times (X / MW\ B_2O_3) \times MW\ H_3BO_3 + Y$$

From the simultaneous solution of this equation and the equation X + Y = 10 g, X and Y were calculated as 2.259 and 7.741 respectively. This simple experiment indicated that $B_2O_3$ to be used in this experiment was actually 22.59% $B_2O_3$ and 77.41% $H_3BO_3$. This powder could be calcined before using but the powder was used without calcination to find whether $TiB_2$ could be produced from $H_3BO_3$ directly. The ceramic mixture was produced by this method and the aluminum matrix was prepared from commercial purity Al ( purity > 99.5%) in the form of wires and commercial purity Mg ingots ( purity > 99.5%).

### 3.3 Production of the Ceramic Powder

Appropriate amounts of $TiO_2$, $B_2O_3$ and Al powders to add up to 30 grams as determined from the stoichiometry of the reaction taking into account of the amount of conversion of $B_2O_3$ into $H_3BO_3$ were weighed and mixed into alcohol to ensure homogeneity and then dried. Pellets were prepared by pressing the dried powder in a die using a pressure of 15 – 20 tons. The pellets were then placed in a preheated furnace heated to 1000ºC in graphite crucibles. After keeping the pellets at 1000ºC for 1 hour it was removed from thr furnace and cooled. The pellets were observed to retain their original shapes (although dimensions have changed and some swelling has taken place) and they could easily be removed from the graphite crucible. The product was in porous form. The porous reaction product is analysed by SEM to determine the phases present with the aid of EDS analysis. The pellets were then crushed into smaller particles and then ground using a rotatory mill. The holding time in the mill varies but it is around 3 minutes. After that, to remove any excess boric oxide that might have remained in the pellet due tothe use of excess $B_2O_3$ in the preparation of the pellet, the powder was mixed with pure water, was filtered using filter paper and then dried. Final powder was analyzed with X – Ray diffraction in order to detect if the reaction went into completion and correct phases were present. Finally, after obtaining enough amount of powder using the process described above, particle size distribution was determined by mesh analysis.

### 3.4 Casting of the Metal Matrix Composites

Melting of the matrix alloy was performed by an inductotherm induction furnace. 1 kg of aluminum wire was melt in the furnace at a temperature of about 700°C. Then 20 g of Mg was added into the melt and alloying is completed. In earlier studies, the ceramic powder was first introduced into the melt using the gas injection apparatus which is used in the study of Elmadağlı [65]. However, it is observed that this apparatus is not working properly, mainly due to the escape of fine particles before melting. Because of this, it is decided in this study that the

particles would be added manually on the top of the melt. By doing so, the powder was added into the melt by pouring on the top and then stirring vigorously to incorporate the particles into the melt. As it will be discussed in chapter IV, particle incorporation occured in steps before all particles are incorporated into the melt. After particle incorporation, slag was removed. Afterwards, near net shape cast specimens were produced using a hydraulic pressure casting machine. The steel mold was preheated before casting by the help of flame. The pressure casting machine makes it available to get tensile test and hardness test samples by the shape of the steel mold inside. Examples of these samples is given in figure 40. For each casting, the casting and pressurizing operation was repeated several times to obtain enough amount of tensile and hardness test samples. The casting was air cooled. After that, test samples were removed from the main body of the casting and the sharp corners were roughly cleaned. The sides of these samples were further polished by boring tool. The hardness test sample surfaces are polished by SiC polishing paper to produce a clean surface.

**Figure 40. 1x1 photo of tensile test and hardness test samples**

### 3.5 Metallographic Examination

Samples taken from the hardness test samples were subjected to metallographic examination. The sample surfaces were ground using SiC grinding papers of size 220, 400, 800 and 1200. Right after, they were polished with alumina solution.

Finally, they were etched using Keller's and Tucker's reagent which Tucker's reagent is a more concentrated version of Keller's reagent. The samples were examined by optical microscope and then photographed. The grain size was measured using linear intercept method on these photographs. On the same polished samples, SEM analysis was performed, obtaining SEM images of reinforced samples. In addition to these, EDXA (Energy Dispersive X – Ray Analysis) analysis was also performed to determine the phases present in the composite.

### 3.6 Mechanical Testing

Tensile tests were carried out at room temperature using an Alşa mark tensile tester. The Ultimate Tensile Strength, Yield Strength, % Elongation and % Area Reduction was calculated for each casting containing 3 samples and these values were averaged to obtain the values for each casting (sample 1, sample 2, sample 3 and sample 4).

Hardness test was carried out by using a hardness tester with ball diameter 2.5 mm and 15 kg load. For each casting (sample 1, 2,3,4) 9 Brinell Hardness values were obtained and these were averaged to obtain the hardness value for each casting. The results are presented in Chapter IV.

# CHAPTER IV

## RESULTS AND DISCUSSION

### 4.1 Production of $TiB_2 – Al_2O_3$ Powder Mixture

Pellets prepared from $B_2O_3$ ($H_3BO_3$) – $TiO_2$ – Al powders were placed into a furnace heated to 1000C in graphite crucibles. The expected overall reaction is:

$$3\ TiO_2 + 3\ B_2O_3 + 10\ Al = 5\ Al_2O_3 + 3\ TiB_2$$

The B2O3 used in this experiment was actually a mixture of $B_2O_3$ and $H_3BO_3$ as stated in the previous chapter. In the calculation of the stoichiometric weight of $B_2O_3$, the $B_2O_3$ – $H_3BO_3$ mixture was first assumed as 100% $B_2O_3$ when the quantity of $B_2O_3$ becomes less than the stoichiometric amount, and it was then taken as 100% $H_3BO_3$ when the quantity of $B_2O_3$ becomes more than the required stoichiometric amount.

After keeping the pellets at 1000C for 1 hour they were removed from the furnace and cooled. The reaction products were subjected to XRD after grinding. The reaction products obtained from pellets in which the amount of $B_2O_3$ was more than the stoichiometric amount were subjected to water to dissolve the excess unreacted $B_2O_3$. The only peaks in the XRD pattern of such a reaction product, shown in figure 41 are those of $TiB_2$ and $Al_2O_3$ indicating complete reaction.

In the case where the amount of $B_2O_3$ is less than the stoichiometrically required amount, it is seen that there is the presence of $Al_3Ti$ in the product powder. The X – Ray pattern illustrating this situation is given in figure 42.

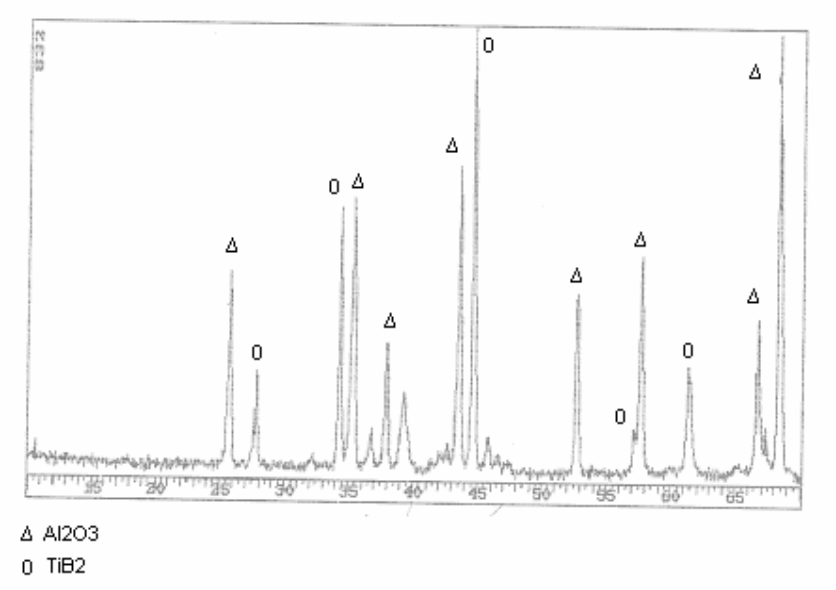


**Figure 41. X-Ray Diffraction pattern for the ceramic powder**

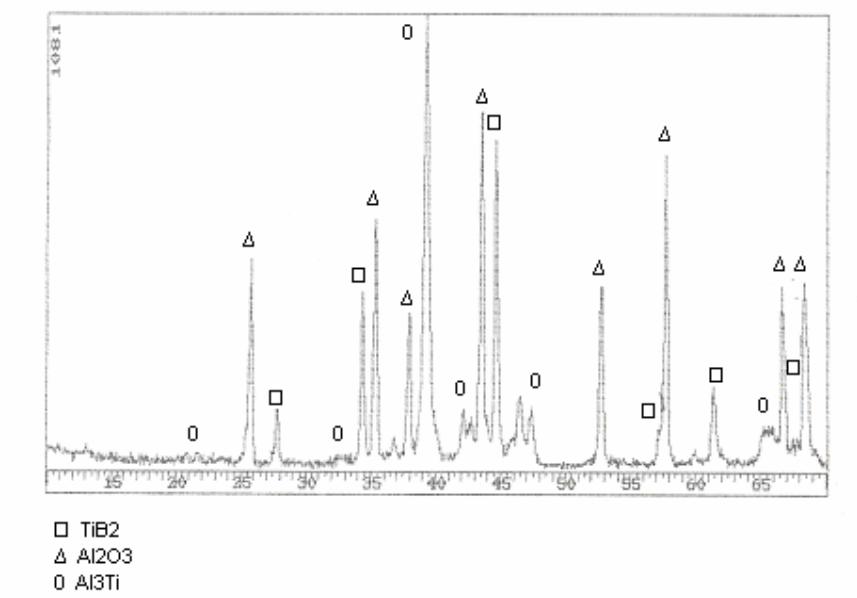


**Figure 42. X – Ray Diffraction pattern showing $Al_3Ti$ peaks which indicates incomplete reaction**

In the study by Sundaram et al. [16], instead of $Al_3Ti$, $AlTi_3$ formation is detected by the x–ray analysis of the product from two component mixtures of reactants which gave them an idea about the mechanism of the reaction. Their proposed mechanism is given in part 2.3 of this study. It is seen that there is a difference in the intermediate reaction product formation of this study and theirs . This difference of the intermediate products formed during the reaction is interesting and it led us in this study to propose a different mechanism. Before doing so, another work [45] was helpful to examine, where in this work, in situ formed $Al_2O_3$, $TiB_2$ and $Al_3Ti$ mixture reinforced aluminum matrix composites is produced by reaction sintering from reactants Al, $TiO_2$ and B. In this study, it has been observed that the amount of $Al_3Ti$ is reduced by increasing the B content, which indicates that $Al_3Ti$ is an intermediate reaction product obtained from the reaction between $TiO_2$ and Al. After this, replacing $AlTi_3$ with $Al_3Ti$ as an intermediate product also depending on this study, we proposed asnother mechanism which is given below:

$$3\ TiO_2 + 13\ Al = 3\ Al_3Ti + 2\ Al_2O_3$$
$$3\ B_2O_3 + 6\ Al = 3\ Al_2O_3 + 6B$$
$$3\ Al_3Ti + 6\ B = 3\ TiB_2 + 9\ Al$$

---

$$3\ TiO_2 + 3\ B_2O_3 + 10\ Al = 5\ Al_2O_3 + 3\ TiB_2$$

The reaction pellets were held in the furnace for one hour. Actually the reaction can proceed at 298°K if it is ignited properly as it produces a local heat zone reaching high adiabatic flame temperatures but the length of the holding time was high in order to reduce boric acid which might take time.

The reaction product is in the form of loose packed pellets. Previous work by Elmadağlı [46] indicates microscopic phase seperation where several micron sized

$TiB_2$ particles are observed to disperse in the $Al_2O_3$ matrix using SEM and EDS analysis. In this work, an attempt was made by using SEM and EDS, but no distinct separation of phases which is mostly indicated by the different color schemes of the phases (dark and light) could be detected. The SEM photograph is given in figure 43 and the EDS analyses of points 1, 2 and 3 on figure 42 are given in figures 44,45 and 46.

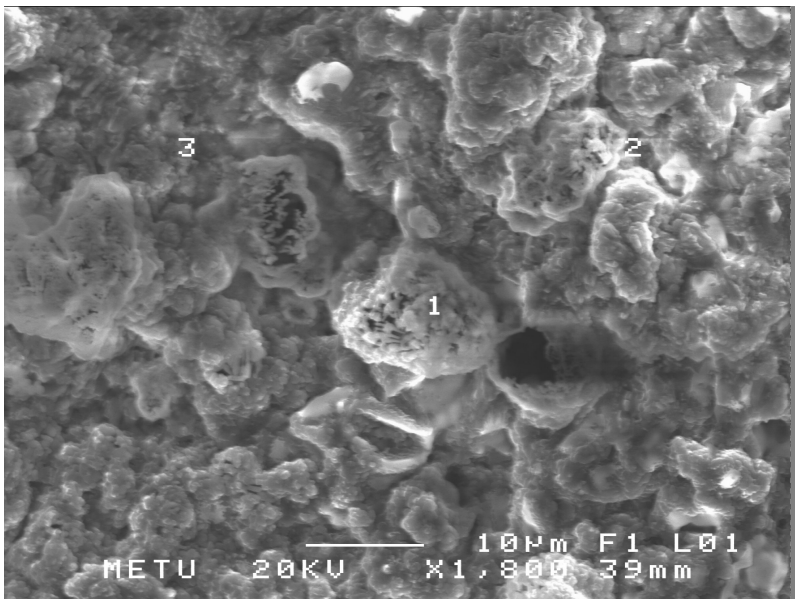


**Figure 43. SEM image of the porous reaction product**

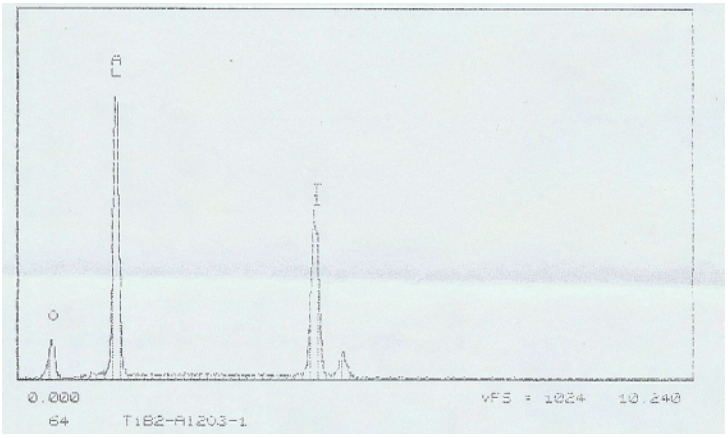


**Figure 44. EDS plot of point 1 in figure 3**

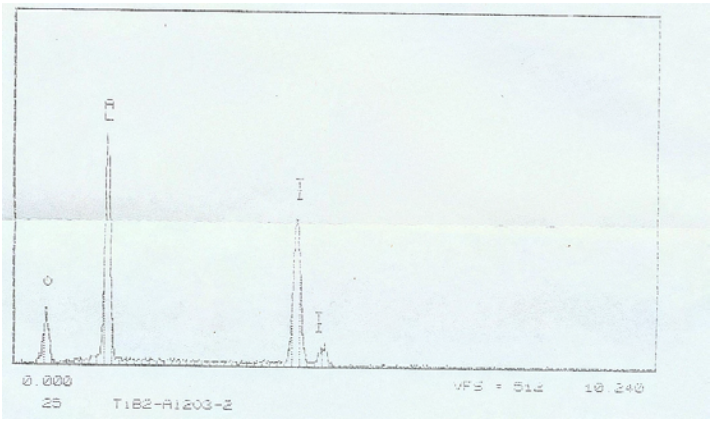


**Figure 45. EDS plot of point 2 in figure 3**

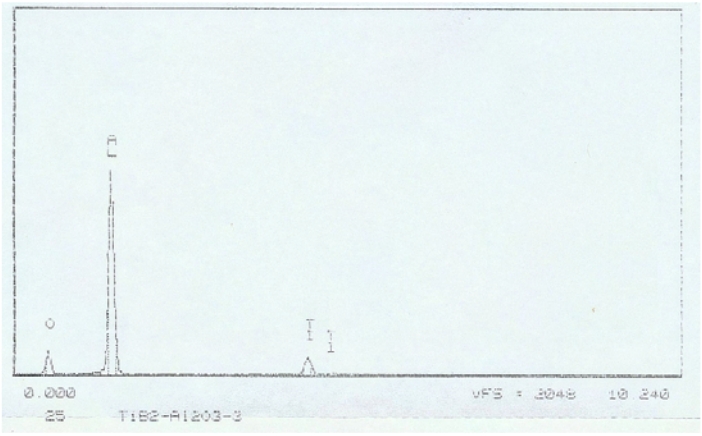


**Figure 46. EDS plot of point 3 in figure 3**

Observing the SEM image, some light colored areas can be seen but the distinction between the dark phase and the light phase is not very obvious. Nevertheless, this might still give us the idea that phase seperation is on the microscopic scale in some degree but definitely not on the macroscopic scale. Thus physical seperation of $TiB_2$ from $Al_2O_3$ is difficult.

### 4.2 Particle Incorporation

The mechanism of particle incorporation is shown in figure 47. Particles first make lumps on the surface. These lumps then incorporate to the liquid and then they disperse. It is indicated elsewhere [47] that there is an incubation period after there is an abrupt increase in the amount of particle incorporation. It can be said that this is also observed in this study.

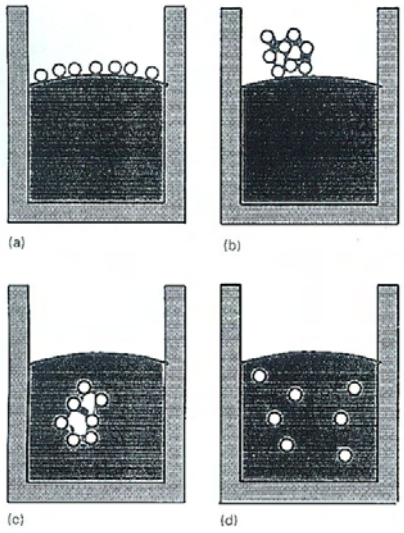


**Figure 47. Figure showing the incorporation mechanism of particles to the melt: a) Addition of particles b) Lumping of particles on the melt surface c) Incorporation of the lump into the melt d) Dispersion of the lump inside the melt**

The particles were added on the top of the melt when the melt was around 700°C and vigorous stirring by a a graphite rod was applied. It is a certain fact that both ceramics are not wet spontaneously by the melt alloy although it is known that addition of Mg significantly lowers the contact angle. In all cases, mechanical or other kind of work is required for the particles to be incorporated in the liquid. This is due to a surface tension barrier which is explained in schematically in part 2.4.3 of this study. It will be seen in part 4.4 of this section that the dispersion of

particles is fine but there is some porosity present in the final parts. In the similar study of Elmadağlı [46], there is no porosity present as the particles are injected under the melt surface by Argon as carrier gas but this time the dispersion of particles is not well and agglomerates are present. This is because fine sized particles escaped the melt by the reflecting gas from the melt. Reducing the gas pressure does solve this problem but this time homogeneous mixing can not be achieved due to the lower gas pressures so as a result, particle agglomeration is observed in this study. Thus, he calculated particle yields from density measurements and concluded that particle yield is high. In the present study, it is assumed that particle yield is maximum as all particles are added on the top of melt and all of them incorporate in the liquid.

### 4.3 Solidification

Solidification and its parameters are important in determining particle engulfment or rejection in the melt. In this study, it was observed that nearly all particles were rejected. This is consistent with the fact that in Al – 3Mg alloys reinforced with $Al_2O_3$ or $TiB_2$, at all growth conditions, particles are rejected which is also indicated in part 2.5 of this study. Nevertheless, one might want to discuss the parameters affecting particle engulfment or rejection. Even if there is a critical velocity above which particles are engulfed, it is known that for most conventional casting processes including the process in this study, this velocity is overcomed. Another important factor is the convection level in the liquid. It is known that reinforced alloys have grain sizes above their unreinforced counterparts as particles hinder the convection of liquid. However in the presence of grain refiners which either reduce the grain size by heat transfer or by promoting nucleation of the matrix by catalysis, grain sizes below the unreinforced alloy can be obtained in the composite. In this study, grain size of the reinforced samples (sample 2 and sample 3) is lower than the grain size of the unreinforced sample (sample 1) which is due to the grain refining effect of $TiB_2$. Together with this, when the dendrite arm spacing is smaller than the particle size, one can not differentiate if particles are rejected or they are mechanically interlocked between dendrite arms. Agglomerate

formation is also associated with high convection level in the melt and the particle size. When the particle size is fine, under high convection levels, particle agglomeration is expected. The particle distribution and grain size effects is discussed in the following parts of this section, part 4.4 and 4.5. .

### 4.4 Microstructure

The optical photographs showing the microstructure of the unreinforced alloy (sample 1), 3.54 vol% reinforced alloy (sample 2) and 5.84 vol% reinforced alloy (sample 3) are given in figures 48, 49 and 50. From the figures of reinforced alloys, it can be seen that particles are uniformly distributed, but they are located between the dendritic structures or grains. It can also be roughly observed that the grain size is smaller in reinforced alloys (sample 2 and 3). Some porosity is also seen, and size of these pores are nearly the same. It is known that reinforced alloys have a greater tendency for porosity, and it is observed in this study that amount of porosity in reinforced alloys is higher than the porosity of the unreinforced ones. As quoted by reference 38, $TiB_2$ grain refiner particles provides nucleation sites for pores without influencing interfacial tension which controls pore size. It is also reported that percent porosity is actually reduced in the case when Mg is present together with grain refiner $TiB_2$ but in the case of this study, the other reinforcement $Al_2O_3$ seems to have an effect on percent porosity. Also when pressure casting is used instead of mould casting, porosity is significantly reduced. This can be illustrated by figures 51 and 52, which are the optical photographs of

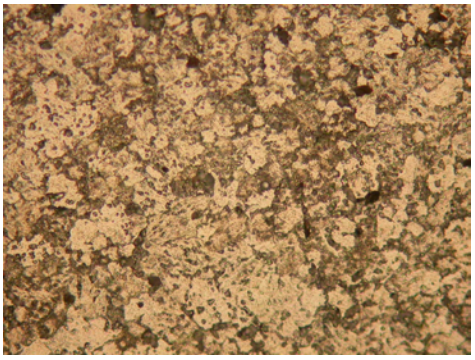

**Figure 48. Microstructure of the unreinforced alloy (sample 1) x 200**

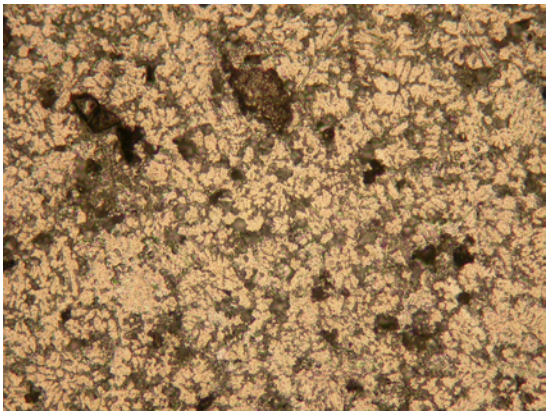

**Figure 49. Microstructure of 3.54 vol% reinforced alloy (sample 2) x 200**

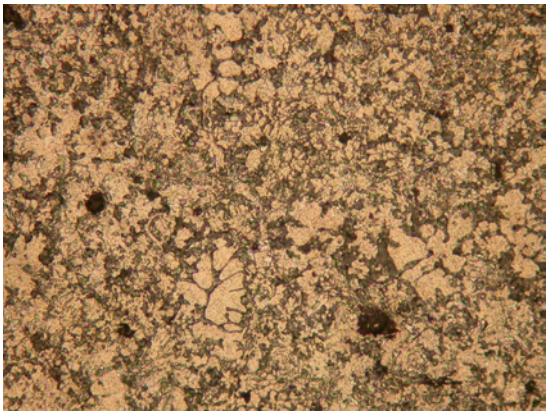

**Figure 50. Microstructure of 5.84 vol% reinforced alloy (sample 3) x 200**

samples taken from a graphite mould casting and pressure casting. It can be seen that the pore size in the case of graphite mold casting is significantly higher than in the case of pressure casting.

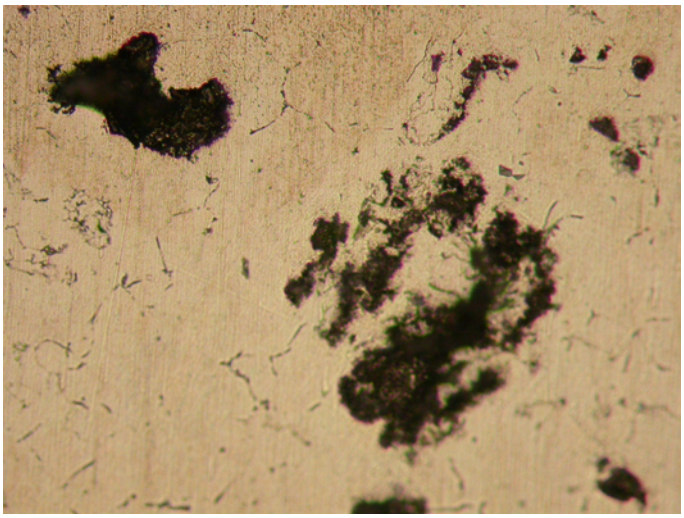

**Figure 51. Microstructure of sample poured into a graphite mold showing porosity, x 200**

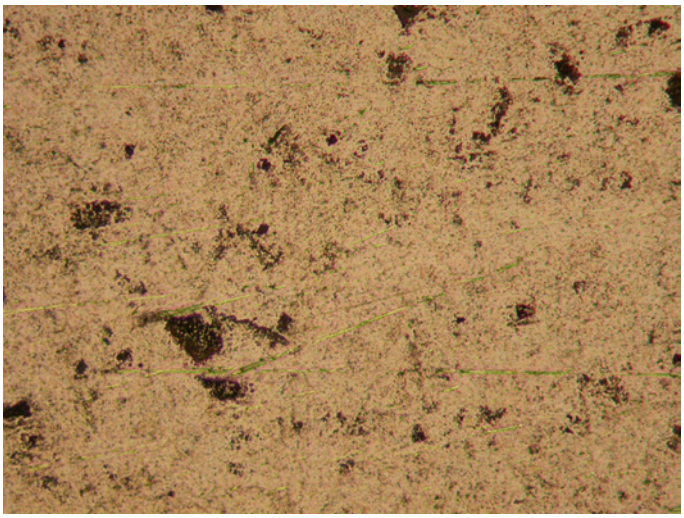

**Figure 52. Microstructure of sample produced by pressure casting showing porosity, x 200**

SEM images of 3.54 vol% reinforced alloy (sample 2) and 5.84 vol% reinforced alloy (sample 3) is given in figures 53 and 54. These also indicate that reinforcement distribution is uniform and they are located primarily in the interdendritic regions.

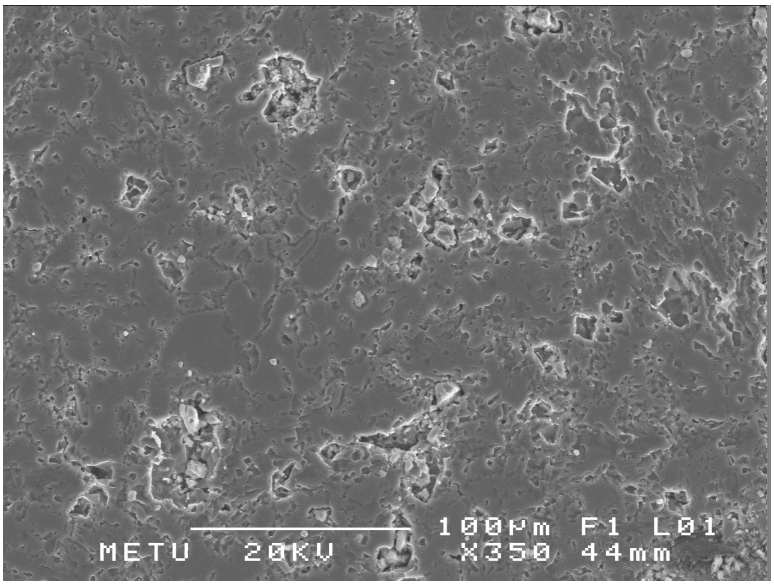


**Figure 53. SEM image of 3.54 vol% reinforced alloy (sample 2)**

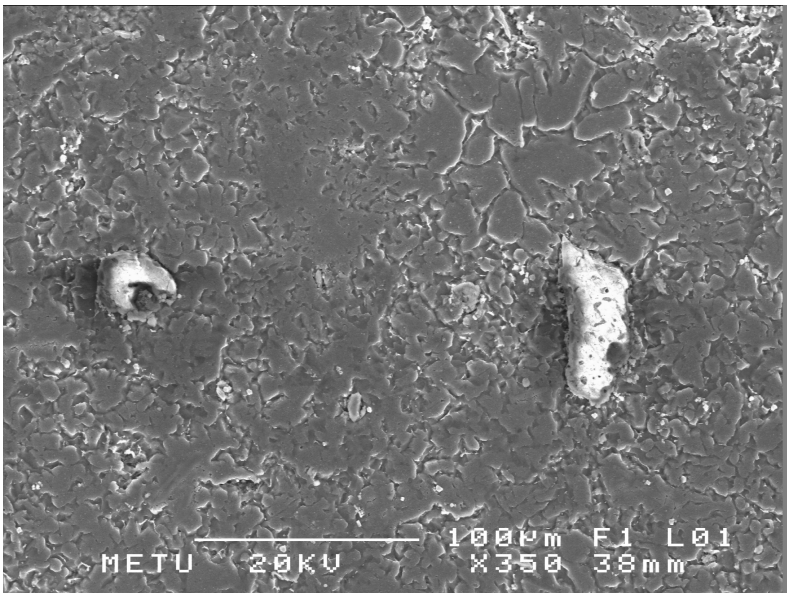


**Figure 54. SEM image of 5.84 vol% reinforced alloy (sample 3)**.

### 4.5 Mechanical Testing

The mechanical testing results are given below:

**Table 1. Mechanical Testing Results of Samples**

| Sample | Sample 1 | Sample 2 | Sample 3 | Sample 4 |
|---|---|---|---|---|
| **Vol% Reinforcement** | 0 | 3.54 | 5.84 | 5.84 |
| **0.2% YS (MPa)** | 60.32 | - | - | 70.07 |
| **Change %** | - | - | - | 16.16 |
| **UTS (MPa)** | 150 | 164.17 | 153.7 | 154.35 |
| **Change %** | - | +9.45 | +2.46 | +2.90 |
| **% Elongation** | 13.47 | 10.31 | 11.66 | 9.65 |
| **Change %** | - | -23.45 | -13.44 | -28.35 |
| **% Area Reduction** | 24.74 | 16.7 | 20.71 | 12.16 |
| **Change %** | - | -32.5 | -16.28 | -50.84 |
| **BHN** | 39,12 | 53.05 | 44.51 | 51.16 |
| **Change %** | - | +35.61 | +13.77 | +30.77 |

These results are illustrated graphically in figures 55, 56, 57 and 58. According to these, it is observed that while UTS and hardness of reinforced alloys (sample 2 and 3) increased with respect to unreinforced alloy (sample 1), % Elongation and % Area reduction decreased. The increase in strength and hardness is due to the addition of particles which is represented by the increase in UTS and BHN. The decrease in ductility which is represented by the decrease in % Elongation and % Area Reduction can be attributed to the stress concentration on the sharp edges and corners of reinforcement particles. The shape of the particles is angular and if they

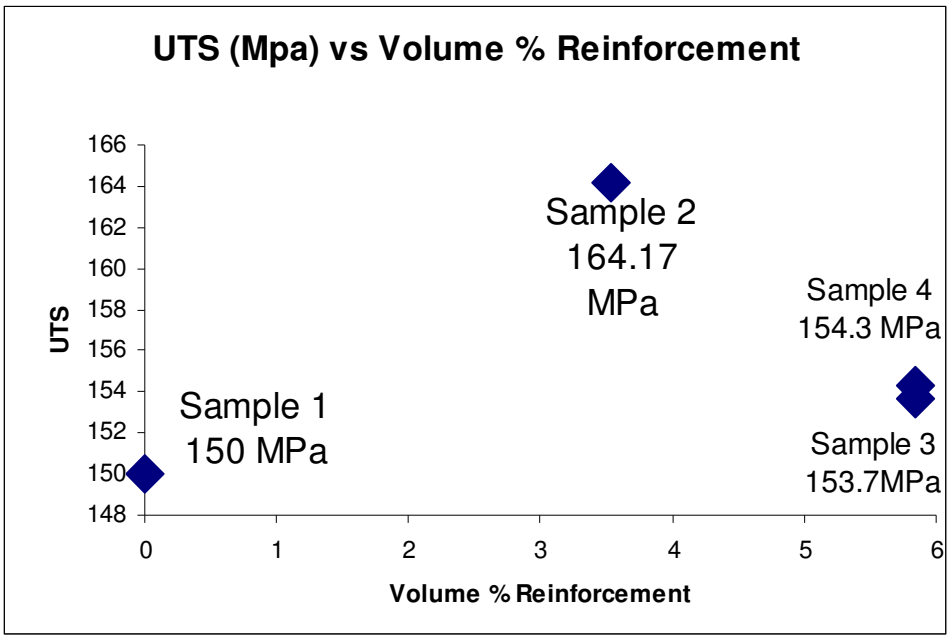


**Figure 55. Plot showing UTS vs vol % reinforcement of samples 1,2,3 and 4**

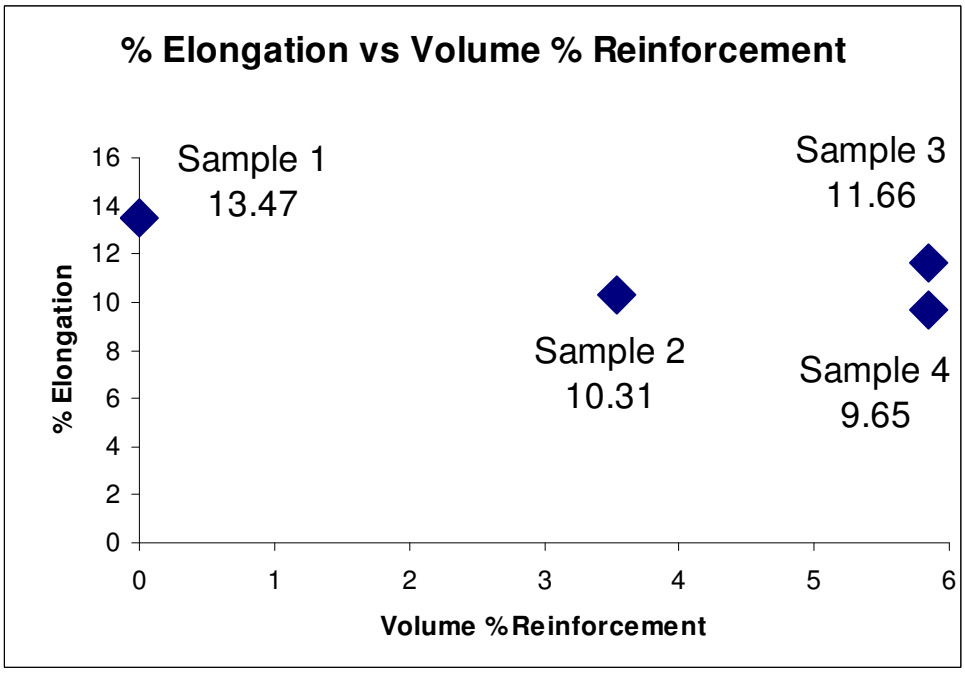


**Figure 56. Plot showing % Elongation vs vol % reinforcement of samples 1,2,3 and 4**

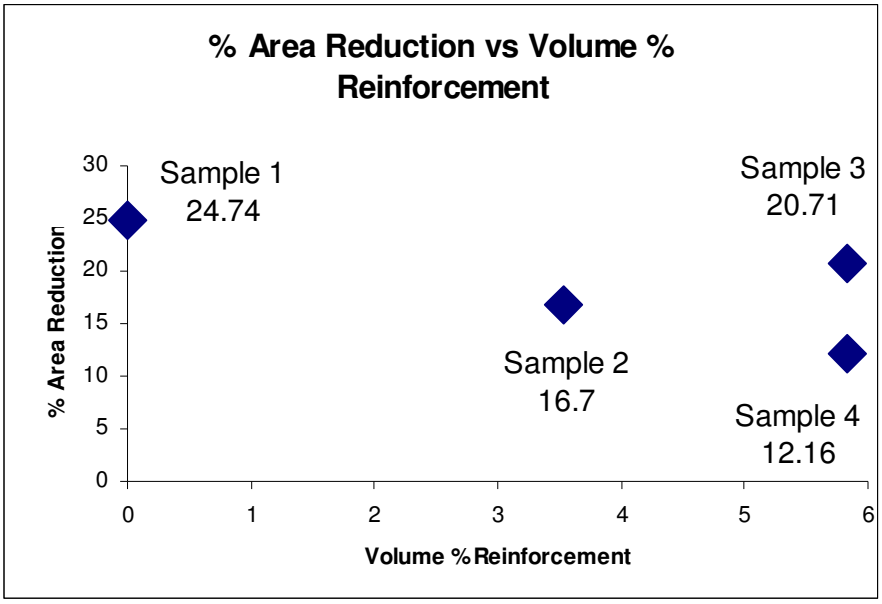


**Figure 57. Plot showing % Area Reduction vs vol % reinforcement of samples 1, 2, 3 and 4**

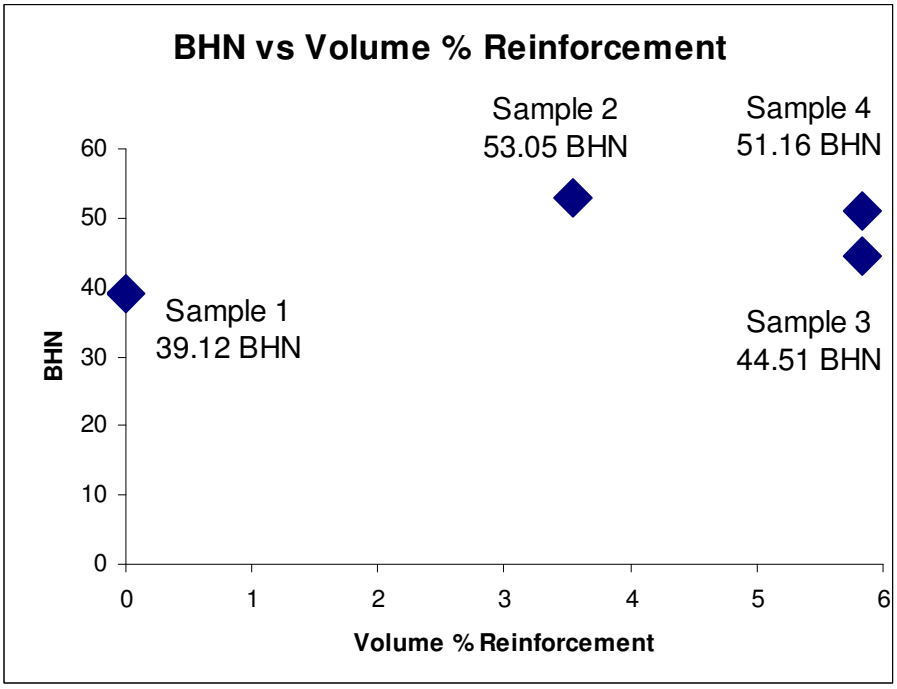


**Figure 58. Plot showing BHN vs vol % reinforcement of samples 1, 2 and 3**

were spherical the ductility would be higher as loading would be concentrated more on the matrix instead of the reinforcement.

Although strength increased and ductility decreased with addition of particles, this increase is lower in the case of 5.84 vol% reinforced alloys (sample 3 and 4). This is related to the particle size of the reinforcement in this case. The particle size distribution is given below for sample 3 and 4 in tables 2 and 3:

**Table 2. Particle size distribution of sample 3**

| **Sample 3** | |
|---|---|
| **Weight percent** | **Particle Size (μ)** |
| 3.95 | < 38 |
| 25 | 38 – 45 |
| 23.68 | 45 – 63 |
| 18.42 | 63 – 90 |
| 17.1 | 90 – 125 |
| 7.9 | 125 – 150 |
| 3.95 | > 150 |

**Table 3. Particle size distribution of sample 4**

| **Sample 4** | |
|---|---|
| **Weight Percent** | **Particle Size (μ)** |
| 8.33 | 38 – 45 |
| 50 | 45 – 63 |
| 37.5 | 63 – 90 |
| 4.17 | 90 – 125 |

From this data, it is seen that the particle size distribution of sample 4 has finer particles when compared to sample 3. For sample 3, it can be seen from the distribution that 28.95 wt% of the particles added is above 90 μm. This can also be illustrated by the SEM image of this sample given in figure 57. In this figure, particles of size well above 90 μm can be seen. This coarse particle size led to a decrease in the strength of the composite. The slight increase of strength of sample 4 compared to sample 3 (both have same volume percentage of particles) is an illustration of the effect of particle size on tensile strength. The reason of this depends on the Weibull distribution of cracks which is explained in part 2.8 of this study. Sample 4 is observed metallographically and it is also seen that porosity is much higher than it is in sample 3. This might also have caused a decrease in strength and this clearly indicates that, the particle size difference led a higher increase in strength than it is assumed.

In general, the strengthening mechanisms in particulate reinforced metals are given in part 2.9 of this study. The first mechanism is given as quench strengthening which is also illustrated in figure 59 . This is due to the mismatch of CTE of the alloy and the ceramic as a result of which a subgrain structure is formed generating high dislocation densities around particles. This can be formulated as indicated in equation 10 in part 2.9:

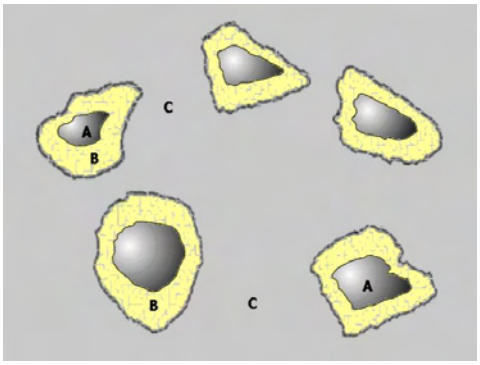


**Figure 59. Schematic diagram illustrating quench strengthening: A: Reinforcement, B: Strain hardened zone with high dislocation density, C: Elastic zone**

$$\sigma_d = \alpha G b \rho^{1/2}$$

$$\rho = 12 \Delta T \Delta C F_v / b d$$

**$\sigma_d$ = Strength (0.2% offset yield strength)**

**$\alpha$ = A constant between 0.5 and 1**

**G = Materials shear modulus**

**b = burger's vector**

**$\rho$ = Dislocation density**

**d = Reinforcement size**

**$F_V$ = Reinforcement volume fraction**

**$\Delta C$ = Product of the thermal mismatch**

**$\Delta T$ = Temperature change**

**Equation 10**

This analysis assumes that dislocations are uniformly distributed and all dislocations contribute to the strength.

The second mechanism is grain strengthening which results from the grain refining effect of particles producing a grain size considerably smaller than the unreinforced matrix alloy. This effect is formulated by the Hall-Petch relationship which is originally developed for describing the strengthening due to the pinning of the dislocations at the grain boundaries. Nevertheless, it is assumed that it can be used effectively in particle reinforced metals. The equation is as follows as indicated by equation 11 in part 2.9:

$$\sigma_0 = \sigma_i + k\, D^{-1/2}$$

**$\sigma_0$ = Yield stress**

**$\sigma_i$ = The friction stress representing the overall resistance of the lattice to dislocation movement**

**k = The locking parameter which gives a measure of the relative hardening condition of the grain boundaries**

**D = Grain diameter**

**Equation 11**

The 0.2% offset yield strengths of unreinforced alloy (sample 1) and sample 4 are 60.32 MPa and 70.07 MPa from mechanical testing results. The grain sizes of the unreinforced alloy (sample 1) and 5.84 vol% reinforced alloy (sample 4) is calculated using linear intercept method. They are 111.63 μm and 99.07μm respectively. The average particle size of sample 4 is calculated from the particle size distribution of this sample and it is found to be 63.63μm. In the first equation, typical values for α, G and b are 0.75, 23 GPa and 0.28 nm. The temperature change ΔT is approximately 500. CTE for Al, $TiB_2$ and $Al_2O_3$ are 24, 8.2 and 7.9 μm/K. In the second equation, typical value for k is 50 Mpa $\mu m^{1/2}$ . Using these values and above equations, yield strength of 5.84 vol% reinforced alloy (sample 4) is predicted in two steps. The contribution of grain size effect is calculated using the formula below:μ

$$\Delta\sigma_1 = k\,(\,1 / D_f \;-\; 1 / D_i\,)$$

$D_f$ = 99.07μm

$D_i$ = 111.63μm

The contribution from grain strengthening is found to be 0.056 MPa. The other contribution is found by putting appropriate values which are given in the above paragraph into the first equation and it is equal to:

**$\Delta\sigma_2$ = 9.378 MPa**

These two contributions make a total of $\Delta\sigma$ = 9.434 MPa. When this contribution is added to the experimental yield strength value of sample 1, it makes 69.754 MPa and this value is very close to the experimental yield strength value of sample 4 which is 70.07 MPa.

Finally, comparison of the UTS and % Elongation values for the 3.54 vol% reinforced alloy (sample 2) with composites produced by some other methods is given below in table 4. While comparing these values, it must be noted that in some methods, the specimens were extruded or heat treated. This adds up on the strength. Nevertheless, it can be said that UTS value of 3.54 vol% reinforced alloy (sample 2) is comparable to these values. Especially % Elongation to failure of sample 2 is well above other composites, which is a positive situation.

**Table 4. Comparison of mechanical test results of the present study with other studies**

| Process | Vol % (Wt%) Reinforcement | UTS (MPa) | % Elongation to failure |
|---|---|---|---|
| **$Al_2O_3$, $TiB_2$ composite formed by melt-stirring (Present Work)** | 3.54 vol% total $Al_2O_3$ and $TiB_2$ / Al | 164.17 | 10.31 |
| **In-Situ formed $Al_2O_3$ and $TiB_2$ reinforced composite [45]** | 10.5% vol% $Al_2O_3$, 9.5 vol% $TiB_2$ / Al | 381.16 | 5.53 |
| **Pressureless Infiltration formed $Al_2O_3$ reinforced Composite [48]** | 58 vol % $Al_2O_3$ / Al | 457 | 0.476 |
| **Reaction Pressing formed $TiB_2$ reinforced composite [49]** | 20 Vol % $TiB_2$ / Al | 334 | 7 |
| **In-Situ (Stir cast) formed $TiB_2$ reinforced composite [50]** | 7.3 Vol% $TiB_2$ / Al | 164 | 6.3 |
| **In – Situ composite Synthesized by stir cast route [51]** | 15 Vol% TiB2 / Al | 223.5 | 4.6 |
| **Duralcan process formed $Al_2O_3$ reinforced Composite (T6) [35]** | 10 Vol % $Al_2O_3$ / Al | 352 | 10 |

# CHAPTER V

## CONCLUSION

So far, the experiments show that a MMC made up of aluminum matrix and $Al_2O_3$ and $TiB_2$ ceramic powder reinforcement can be succesfully produced. If it is summarized, first of all the reinforcement can be obtained by means of the thermite reaction between reactants Al, $TiO_2$ and Boric Acid. Although the common reactants include $B_2O_3$ instead of Boric Acid, it is shown by this study that the reinforcement mixture can be obtained by using Boric Acid instead of $B_2O_3$ by simply adjusting the stoichiometry of the reaction and increasing the furnace time. It is believed that this cheap production of reinforcement can be improved by determining the minimum time in the furnace although there has not been an attempt made for this in the present study.

Second, the casting of the composite using the reinforcement mixture and commercial purity aluminum has been succesfull in terms of the mechanical properties . However, it can be said that melt stirring method can be improved by finding a means for reducing the gas entrapment and enhancing homogeneous mixing.

This study is different from similar studies in a way that the reinforcement in other studies is either $Al_2O_3$ or $TiB_2$ alone. This somehow makes the comparison of the present study with these difficult but in general all can be considered similar. Then, some literature survey on basic phenomena governing all of these studies is presented in this study such as wetting and solidification. It is believed that at least these can be helpful to others as they can find a summary of these phenomena as well as the necessary sources to obtain further information on them.

Finally, it is thought that the method used in this study can be applied to produce a MMC with desired mechanical properties succesfully.

# REFERENCES

[1] Chawla, Krishan Kumar, Composite Materials: Science and Engineering, pg. 165 – 168

[2] Maxim L. Seleznev, Igor L. Seleznev, James A. Cornie, Ali S. Argon, Ralph P. Mason, SAE International Congress and Exposition Detroit, MI February 23 – 26, 1998, Paper 980700

[3] Low Cost Aluminum Metal Matrix Composite Materials, Warren H. Hunt, http://www.almmc.com/UserResourceCtr/Presentations/LowCostAlMMCmaterials, September 10, 2004

[4] Veronique Michaud in Fundamentals of Metal Matrix Composites edited by S. Suresh, A. Mortensen, A. Needleman (1993) pg. 3 – 22

[5] Skibo, M.D., and Schuster D.M., U.S. Patent No. 4,786,467, November 22, 1988

[6] Skibo, M.D., and Schuster D.M., U.S. Patent No. 4,759,995, July 26, 1988

[7] MMC-Assess, H. Peter Degischer, September 10, 2004, http://mmc-assess.tuwien.ac.at/index1.htm

[8] Ilegbusi, O., and Szekely, , J., J. Colloid Interface Sci. (1988) 125, pg 567 – 574

[9] Taheri-Nassaj, E., Kobashi, M., and Choh, T. Scripta Materialia, vol 34 No. 8, (1996) pg. 1257 – 1265

[10] Kobashi, M., Choh, T., Journal of Materials Science Vol. 32 (1997) pg. 6283 – 6289

[11] Mortensen, A. And Jin, I. International Materials Reviews 1992 Vol. 37 No.3 (1992) pg. 101 – 128

[12] Cochran, C.N. and Ray, R.C., U.S. Patent No. 3,547,180, December 15, 1970

[13] Tang, W. And Bergman, B. Materials Science and Engineering, A177 (1994) pg 135 – 142

[14} MMC-Assess, H. Peter Degischer, September 10, 2004, http://mmc-assess.tuwien.ac.at/4/index.htm#B1

[15] Logan K.V., Walton J.D., Ceramic Engineering and Science Proceedings Vol. 5 (1988) pg. 712 – 738

[16] Sundaram, V., Logan, K.V. and Speyer, R.F. Journal of Materials Research, Vol 12 No. 7 pg. 1681 – 1684

[17] Barin I., Knacke O., Thermochemical Properties of Inorganic Substances

[18] Barin I., Thermochemical Data of Pure Substances

[19] Padday J.F Spreading, Wetting and Contact Angles Contact Angle, Wettability and Adhesion in Contact Angle, Wettability and Adhesion Edited by Mittal K.L. (1993) pg. 97 – 108

[20] Delannay F., Froyen L. And Deruyttere A., Journal of Materials Science Vol. 22 (1987) pg. 1 – 16

[21] Shaw D.J, Introduction to Colloid and Surface Chemistry 1991, pg. 70

[22] McDonald J.E. and Eberhart J.G., Transactions of the Metallurgical Society of AIME, Vol. 233, (1965) pg. 512 – 517

[23] Champion J.A., Kene B.J. and Sillwood J.M., Journal of Materials Science, Vol. 4 (1969) pg. 39 – 49

[24] Naidich Y.V., Chubashov Y.N., Ishchuk N.F. and Krakovskii V.P., Powder Metallurgy and Metal Ceramics Vol. 22 (1983) pg. 481 – 483

[25] Kozlova O.B., Suvorov S.A., Refractories Vol. 17 (1976) pg. 763 – 767

[26] Yasinskaya G.A., Powder Metallurgy and Metal Ceramics, Vol. 7 (1966) pg. 557 – 559

[27] John H., Hausner H., Journal of Materials Science Letters Vol. 5 (1986) pg. 549 – 551

[28] Oh S.Y., Cornie J.A. and Russell K.C., Metallurgical Transactions A Vol. 20 (1989) pg. 527 – 532

[29] Oh S.Y., Cornie J.A. and Russell K.C., Ceramic Engineering and Science Proceedings, Vol. 8 (1987) pg. 912 – 936

[30] Bruce R.H., Aspects of the Surface Energy of Ceramics. I – Calculation of Surface Free Energies in Science of Ceramics Edited by Stewart G.H., pg. 359 – 367

[31] Mortensen A., Materials Science and Engineering, Vol. A135 (1991) pg. 1 – 11

[32] Jonas R. Tamala, Cornie James A and Russell Kenneth C., Metallurgical and Materials Transactions A Vol. 26A pg. 1491 – 1497

[33] Humenik M., Kingery W.D., Journal of American Ceramic Society Vol. 37 pg. 18 – 23

[34] Omenyi S.N. and Neumann A.W., Journal of Applied Physics, Vol. 47 No.9 (1976) pg. 3956 – 3962

[35] MMC-Assess, H. Peter Degischer, September 10, 2004, http://mmc-assess.tuwien.ac.at/data/prm/duralcan/aa6061

[36] McLeod A.D. and Gabryel C.M., Metallurgical Transactions A Vol. 23A (1992) pg. 1279 – 1283

[37] Lee J.C., Subramanian K.N., Journal of Materials Science Vol. 29 (1994) pg. 1983 – 1990

[38] Roy N., Samuel A.M. and Samuel F.H., Metallurgical and Materials Transactions A, Vol. 27A (1996) pg. 415 – 429

[39] MMC-Assess, H. Peter Degischer, September 10, 2004, http://mmc-assess.tuwien.ac.at/data/prm/in%20situ

[40] Dieter G.E. Mechanical Metallurgy 1988 pg. 212 – 220

[41] Dieter G.E. Mechanical Metallurgy 1988 pg. 369 – 372

[42] Song S.G., Shi N., Gray III G.T. and Roberts J.A., Metallurgical and Materials Transactions A Vol. 27A (1996) pg. 3739 – 3746

[43] Mummery P., Burdekin N. And Stone I. The Effect of Spatial Distribution of Reinforcement on the Fracture of Particle Reinforced MMC's in Metal Matrix Composites and Metallic Foams Edited by T.W. Clyne, Simancik F (1999) pg. 162 – 167

[44] Miller W.S. and Humphreys F.J., Scripta Metallurgica et Materialia Vol. 25, (1991) pg. 33 – 38

[45] Ma Z.Y., Li J.H., Li S.X., Ning X.G., Lu Y.X, Bi J., Journal of Materials Science Vol. 31 (1996) pg. 741 – 747

[46] Elmadağlı Mustafa, Master Thesis, METU, ANKARA, July 2000

[47] Kobashi M., Mohri T., Choh T., Journal of Materials Science Vol. 28 (1993) 5707 – 5712

[48] Aghajanian M.K., Rocazella M.A., Burke J.T. and Keck S.D., Journal of Materials Science Vol. 26 (1991) pg. 447 – 454

[49] Ma Z.Y. and Tjong S.C., Metallurgical and Materials Transactions A Vol. 28A (1997) pg. 1931 – 1942

[50] Tee K.L., Lu L., Lai M.O., Journal of Materials Processing Technology Vol. 89 – 90 (1999) pg. 513 – 519

[51] Tee K.L., Lu L., Lai M.O., Composite Structures Vol. 47 (1999) pg. 589 – 593

[52] Stefanescu D.M., Dhindaw B.K., Kacar S.A. and Moitra A., Metallurgical Transactions A Vol 19A (1988) pg. 2847 – 2855

[53] Donnet J.B., Pure and Applied Chemistry, Vol. 53 (1981) pg. 2223 – 2232